NASA TN D-72

TECHNICAL NOTE

D-72

FULL-SCALE WIND-TUNNEL INVESTIGATION OF THE EFFECTS OF A TARGET-TYPE THRUST REVERSER ON THE LOW-SPEED AERODYNAMIC CHARACTERISTICS OF A SINGLE-ENGINE JET AIRPLANE

By William H. Tolhurst, Jr., Mark W. Kelly, and Richard K. Greif

Ames Research Center
Moffett Field, Calif.

NATIONAL AERONAUTICS AND SPACE ADMINISTRATION

WASHINGTON

September 1959

NATIONAL AERONAUTICS AND SPACE ADMINIS

TECHNICAL NOTE D-72

FULL-SCALE WIND-TUNNEL INVESTIGATION OF THE EFFECTS OF A TARGET-TYPE THRUST REVERSER ON THE LOW-SPEED AERODYNAMIC CHARACTERISTICS OF A SINGLE-ENGINE JET AIRPLANE

By William H. Tolhurst, Jr., Mark W. Kelly, and Richard K. Greif

SUMMARY

Full-scale wind-tunnel tests have been conducted to determine the effects of a semicylindrical target-type thrust reverser on the static stability and control characteristics of a single-engine jet airplane.

The results are presented in the form of three-component force data obtained at Reynolds numbers ranging from 5.8 to 10.1×10^6. Vector-type plots describe the flow angularity and dynamic-pressure ratio in probable horizontal tail locations. Additional data are presented which show the effects of reversed exhaust gases on skin temperatures on the fuselage and horizontal tail and also on buffeting of the horizontal tail.

The results indicate that the major effect of reverser operation on airplane stability was a large nose-down pitching moment which, as shown by flow surveys, was due to the reversed gases altering the downwash pattern in the region of the horizontal tail. Under certain conditions of high engine power and low airspeed, skin temperatures reached a maximum of 500° F on the lower surface of the horizontal tail and 240° F at the rear of the fuselage. Buffet accelerations up to 6g were measured near the tip of the horizontal tail for the combination of high reversed thrust and high forward speed. In general, it appeared that the distortion of the flow field around the airplane and the resulting effects on pitching moment and tail buffeting were defined by the ratio of the reversed thrust to the momentum of the free stream.

INTRODUCTION

Considerable interest has been shown in the use of thrust reversers for a braking device to shorten the landing roll of jet aircraft. Also, because of the inherently slow thrust response of jet engines, thrust reversers may be used in flight as thrust modulators to provide more rapid altitude and speed control. A reverser would be useful to provide rapid

deceleration from cruising speed to landing pattern speed and to provide letdown from altitude without excessive build-up of speed. In the landing approach, a fully modulating reverser would provide rapid control of thrust to allow more precise control of flight path and speed for greater accuracy in touching down at a selected point. These advantages were realized in the flight tests reported in reference 1. During these tests, an F-94C airplane equipped with a fully modulating target-type reverser made landings with the engine power set for level flight in the approach condition with the thrust being controlled entirely by the reverser.

To supplement the investigation of reference 1, full-scale tests were conducted in the Ames 40- by 80-foot wind tunnel on an F86-D airplane also equipped with a target-type reverser to determine the effects of the reverser operation on the static stability and control of the airplane. Presented in this report are force data showing the effects of thrust reversal on the pitching-moment characteristics of the airplane and flow-field surveys describing the flow in the region around the rear of the airplane. Also presented are data describing some of the operational problems involved with reversed thrust, such as exhaust gas reingestion, elevation of skin temperatures, and buffeting.

NOTATION

a vertical acceleration of tip of horizontal tail, ft/sec^2

A area, sq ft

b wing span, ft

c wing chord, parallel to plane of symmetry, ft

$\bar{c}$ mean aerodynamic chord, $\dfrac{\int_0^{b/2} c^2 dy}{\int_0^{b/2} c\, dy}$

C_D drag coefficient, $\dfrac{\text{drag}}{q_\infty S}$

C_L lift coefficient, $\dfrac{\text{lift}}{q_\infty S}$

C_m pitching-moment coefficient, $\dfrac{\text{pitching moment}}{q_\infty S \bar{c}}$

ΔC_m increment in pitching moment due to operation of the thrust reverser

F_G gross thrust from engine, lb

g acceleration of gravity, 32.2 ft/sec^2

i_t horizontal tail incidence angle, deg

N percent of engine rated maximum rpm

p static pressure, lb/sq ft

p_t total pressure, lb/sq ft

q dynamic pressure lb/sq ft

S wing area, sq ft

S_t horizontal tail area, sq ft

T temperature, $^{\circ}F$

U velocity, ft/sec

V_{TP} velocity at exit of engine tail pipe, ft/sec

W_t weight of horizontal tail, lb

W_E weight rate of flow of air through engine, lb/sec

α angle of attack, deg

δ_R deflection angle of thrust reverser, measured from vertical plane parallel to plane of symmetry, deg

ϵ angle of downwash, deg

θ temperature ratio, $\frac{\text{free-stream air temperature, } ^{\circ}R}{\text{standard temperature, } ^{\circ}R}$

Subscripts

f fuselage

j jet exit

t tail

u uncorrected

∞ free stream

MODEL AND APPARATUS

The model used in the test was a YF-86D airplane shown in figure 1. A J-34 turbojet engine was used instead of the standard J-47 engine. A thrust reverser similar to the target-type reverser used in reference 1, was mounted as shown in figure 2.

The location of the reverser relative to the rear of the fuselage is shown in figure 2(a). Figure 2(b) shows the details of the reverser construction while figure 2(c) is a photograph of the reverser installation on the airplane.

The target was a semicylinder with partial end plates with the axis of revolution mounted horizontally and normal to the engine thrust axis. It was parted vertically at the airplane plane of symmetry so that each half of the target could be pivoted to various angles of deflection, δ_R, with respect to this plane. These deflection angles were 12°, 23°, 45°, 67°, and 90°. In the open or undeflected position, $\delta_R = 0^\circ$, the jet exhaust passed straight through for forward thrust.

A baffle plate was required in the fuselage around the tail pipe to prevent the reversed exhaust gases from entering the interior of the fuselage.

The flow-field survey was made with the tunnel survey apparatus shown in the photograph in figure 3. A detailed description of the apparatus can be found in reference 2.

INSTRUMENTATION

The thrust of the engine was determined from measurements of tail-pipe total pressure with a fixed probe in the tail-pipe exit. This system was calibrated at zero free-stream velocity by use of the wind-tunnel balance system. Subsequent tests showed that the calibration of gross thrust against tail-pipe total pressure was not affected by free-stream velocity.

Skin-temperature measurements were made with Chromel-Alumel thermocouples fixed to the outer surface of the skin at seven spanwise stations on the lower surface of the horizontal tail and at five points along the fuselage (fig. 2(a)).

The buffet data were measured by accelerometers mounted in the tip caps of the horizontal stabilizer.

TESTS

The investigation covered a range of angles of attack from -2° to $+20^{\circ}$. The Reynolds number, based on the mean aerodynamic chord of 8.08 feet, varied from 5.8 to 10.1×10^{6} which corresponded to free-stream dynamic pressures from 15 to 45 pounds per square foot. The gross thrust of the engine was varied from 2400 pounds forward to 1000 pounds reverse. For most of the tests the vertical plane of the target was normal to the fuselage reference axis; however, the effect of inclining the target 10° above and 10° below this axis also was determined.

The flow surveys were made only at 12° angle of attack and at a free-stream dynamic pressure of 25 pounds per square foot. For these surveys the engine speed was varied only with the target at either the full-forward thrust or full-reverse thrust deflection.

CORRECTIONS

The following corrections for the tunnel-wall effect were made to the force data.

$$\alpha = \alpha_u + 0.611\ C_{I_u}$$

$$C_D = C_{D_u} + 0.0107\ C_{L_u}^{2}$$

$$C_m = C_{m_u} + 0.00762\ C_{L_u} \text{ (for horizontal tail installed)}$$

In the computation of the pitching-moment data, the moment center was chosen to be on the thrust axis of the airplane with the reverser at $\delta_R = 0^{\circ}$, so that any direct effects of the thrust on the pitching moment were eliminated.

The measured downwash angles and airplane angle of attack were corrected for tunnel air-stream inclination and the air-stream inclination due to the presence of the survey apparatus. The correction for tunnel-wall effect on the downwash was

$$\Delta\epsilon = 0.475\ C_L, \text{ deg}$$

RESULTS AND DISCUSSION

Reverser Characteristics and Aerodynamic Effects

Effectiveness of the target-type reverser.- The effect of the reverser on the gross thrust is shown in figure 4. The variation of gross thrust at $q_\infty = 0$ with engine speed corrected to standard temperature is shown for several target deflection angles. Also included in figure 4 are data showing the reversed gross thrust with the reverser at $\delta_R = 90^\circ$ and $q_\infty = 35$ pounds per square foot. These data, which are typical of all values of q_∞ tested, show that reverser effectiveness is not a function of free-stream dynamic pressure.

Increasing the target deflection angle from $\delta_R = 0^\circ$ to $\delta_R = 67^\circ$ reduced the amount of forward thrust. Reversed thrust was not obtained until the reverser was deflected to some angle between $\delta_R = 67^\circ$ and 90°. At $\delta_R = 90^\circ$, the ratio of reverse thrust to forward thrust increased with increasing engine speed from approximately 49 percent to 53 percent.

Effect of thrust reversal on the longitudinal characteristics of the airplane.- In figure 5 the variations of angle of attack, drag coefficient, and pitching-moment coefficient with lift coefficient for the airplane with the horizontal tail installed are presented for various engine speeds and values of free-stream dynamic pressure. These data are presented for $\delta_R = 90^\circ$ since this deflection showed the greatest effects of reversed thrust on the longitudinal characteristics.

The basic data shown in figure 5(c) indicate that with the engine inoperative there was little change in the pitching-moment characteristics due to the reverser installation. However, with the engine operating there was a large nose-down pitching-moment increment for any reversed thrust condition tested. Furthermore, it was determined from variable tail incidence tests that, with the reverser at $\delta_R = 90^\circ$, the horizontal tail could trim the airplane only at a low lift coefficient under the most favorable conditions tested ($q_\infty = 45$ psf, $N/\sqrt{\theta} = 0.58$).

Further examination of figure 5 shows that the manner in which the pitching-moment increment varied with engine speed was different at the various values of q_∞. At $q_\infty = 15$ pounds per square foot (fig. 5(a)), the magnitude of the pitching moment decreased with increasing engine speed, while at the higher values of q_∞ (figs. 5(b), (c), and (d)) the pitching moment increased with increasing engine speed until stall occurred on the horizontal tail. Further increase in engine speed reduced the pitching-moment increment.

The longitudinal characteristics of the airplane with the horizontal tail removed, figure 6, show that nearly all of the increment of pitching moment due to the operation of the reverser was due to the effect of the reversed gases on the horizontal tail and not to direct forces on the reverser.

Correlation of ΔC_m with $-F_G/q_\infty S$.- In figure 5 it was shown that the variation with engine speed of ΔC_m due to thrust reversal was different at different values of q_∞. However, it was reasoned that some parameter could be found which would correlate the major effects of thrust reversal on C_m over a wide range of values of reversed thrust and q_∞. One choice of such a parameter would be the ratio of the momentum of the reversed gases to the momentum of the free-stream air flow, as represented in the dimensionless parameter, $-F_G/q_\infty S$ (see appendix A).

Figure 7 shows the variation of ΔC_m with $-F_G/q_\infty S$ at several values of q_∞. Good correlation was obtained through a range of reversed thrust from 0 to 1000 pounds and a range of q_∞ from 15 to 45 pounds per square foot.

The variation of ΔC_m with increasing values of $-F_G/q_\infty S$ indicates that below $-F_G/q_\infty S$ of about 0.05 the horizontal tail was unstalled since ΔC_m increased with increasing values of $-F_G/q_\infty S$. At higher values, the reversed gases caused the horizontal tail to stall, resulting in decreasing values of ΔC_m.

Since the pitching-moment contribution of the horizontal tail is determined by the angle of attack and dynamic pressure of the local flow field at the horizontal tail, the correlation of ΔC_m with $-F_G/q_\infty S$ shown in figure 7 indicates that the flow field near the tail is determined by $-F_G/q_\infty S$, at least within the scope and accuracy of these tests. This would indicate that it should not be necessary in tests of reversers to duplicate the full-scale engine tail-pipe pressures and temperatures to obtain similarity between the test flow field and the flow field under actual conditions as long as $-F_G/q_\infty S$ is duplicated.

Flow-field surveys.- Figures 8, 9, and 10 show vector-type plots of the downwash angle and dynamic pressure ratio in vertical planes parallel to the plane of symmetry. The angle of the vector is the downwash angle referenced to the horizontal, and the length of the vector is the measure of q_t/q_∞, based on the unit length shown in each figure. An outline of the rear of the airplane is shown to establish the position of the vectors relative to the airplane components and the thrust reverser. The horizontal tail was removed during the survey but is included in outline to show its normal position in the flow field.

The flow survey was made with the thrust reverser deflected to 90° at a free-stream dynamic pressure of 35 pounds per square foot with the airplane at 11.2° angle of attack.

Figure 8 shows the basic flow field near the rear of the fuselage with the engine off. The flow in the vertical plane at the spanwise station shown was typical of all the planes surveyed. The flow near the tail was uniform with a downwash angle of approximately 7°. The length

of the vectors indicates the dynamic pressure ratio to be slightly greater than unity at the tail. The wake from the wing was well below the tail as indicated by the shorter vectors.

Figure 9 shows the vectors in three spanwise planes with the engine at 60-percent rpm and the reverser in the 90° position. The vectors for the inboard spanwise station show a reduction in downwash angle in the region of the leading edge, and show upwash with a pronounced increase in velocity ratio near the trailing edge of the tail. The dotted-line vectors in the region of the thrust reverser indicate an area of totally reversed or extremely turbulent flow wherein the flow velocity and direction were not measurable by the pitot rake. At the midspan plane (fig. 9(b)), the influence of the reversed gases has subsided somewhat. At the outboard plane (fig. 9(c)), the data show little influence of the reversed gases when compared to the engine-off data (fig. 8).

When the engine speed was increased to 90-percent rpm, the entire flow field in the vicinity of the horizontal tail was strongly influenced by the reversed gases as shown in figure 10. The reversed and turbulent flow region extends outward past the midspan plane (fig. 10(b)) and upward above the plane of the horizontal tail. The vectors indicate that the free-stream flow over the position of the major spanwise portion of the tail has been forced around the reversed gas flow giving rise to high upwash angles with low velocity ratios at the leading edge and downwash angles with low velocity ratios at the trailing edge. Even at the outboard plane (fig. 10(c)) the influence of the reversed gases is great enough to reduce the downwash from 7° to approximately 1° to 2°. It is apparent from the flow studies that the location of the horizontal tail in relation to the thrust reverser is in a position that would give large lifting loads on the tail and in some cases the angles were high enough to stall the tail. In general, it may be concluded that on this airplane the position of the horizontal tail relative to the thrust reverser was in a poor location from the stability and control standpoint. If the tail were in a low position relative to the reverser, the flow survey indicated that there would be a pitch-up of the same order of magnitude as the pitch-down on the present airplane. In order to minimize the effect of the reverser on pitching moment, the data indicate a very high tail position, possibly on top of the vertical tail, would be required.

Effect of reverser deflection angle on the pitching-moment increment.- Figure 11 presents a plot of the variation of ΔC_m with change in reverser target deflection angle at a constant lift coefficient for the various engine speeds. There was a small increase in ΔC_m in deflecting the target from the 0° to the 45° position, but from 45° to 90° there was a rapid increase which reached a maximum at the 90° deflection. In contrast, the results of the flight tests reported in reference 1 indicated that the maximum ΔC_m due to the reverser was obtained with the reverser deflected approximately 75°. The difference between the two results may be explained by the location of the F-94C horizontal tail relative to the target. The position of the tail on the F-94C was forward of the position of the tail

on the F-86. Therefore, the reversed gases exerted less change in the flow around the tail, unless there was attachment of the reversed-gas flow on the fuselage. On the F-94C attachment occurred and was greatest when the target was in an intermediate position.

The trim limit line shown in figure 11 indicates that, for the conditions specified, the airplane cannot be trimmed if the reverser deflection is greater than approximately 74°.

Effects of reversed thrust on the lateral and directional characteristics.- There were no steady-state effects on the lateral or directional characteristics which were of a magnitude comparable to the effects of the reversed flow on the longitudinal characteristics. There was, however, a directional oscillation of the airplane which was encountered occasionally at the highest values of $-F_G/q_\infty S$. Tuft studies indicated that these oscillations were encountered only when the reversed gases became attached to and flowed along the fuselage, and that they were associated with a random motion of the point of flow separation on the side of the fuselage. This was a random phenomenon and could not be repeated at will. However, it did occur several times and in one instance the oscillations were violent enough to cause local buckling in the fuselage skin.

Effect of target tilt.- An attempt was made to reduce the large pitching-moment change by tilting the target. The target was tilted upward 10° with respect to the thrust axis and downward the same amount, but, as shown in figure 12, neither configuration was effective.

Operational Problems

Reversed-gas reingestion.- Reingestion of the exhaust gases could be avoided by keeping the tunnel free-stream velocity above 15 knots for all engine powers. Reingestion was encountered once during a static calibration but the rate of increase of engine temperature was slow enough that damage was avoided by reducing engine speed slightly.

Skin temperatures.- The temperatures at the rear of the fuselage and on the horizontal tail were strongly affected by reverser deflection, free-stream velocity, and engine speed. Figure 13 shows a plot of a typical variation of maximum temperatures on the fuselage and horizontal tail with changes in reverser deflection. At reverser deflection angles from 0° to 45°, the maximum temperatures were 175° F or less with the fuselage temperatures being higher than the tail lower surface temperatures. At the 67° deflection angle, however, the fuselage maximum temperature was 240° F while the tail lower surface temperature was 500° F. Increasing the reverser to 90° reduced these temperatures again to values in the low temperature range.

Figure 14 shows the variation in temperature with changes in free-stream velocity for two engine speeds at full reverse. At $q_\infty = 0$ the temperatures on the horizontal tail are high and very nearly equal for both 77- and 87-percent rpm. Increasing q_∞ decreased the temperatures immediately for the 77-percent-rpm condition; whereas the temperatures for the 87-percent condition persisted at the high level until $q_\infty = 15$ psf and then decreased. At $q_\infty = 45$ psf, the temperatures at both engine speeds are well below 200° F. In contrast to the temperatures on the horizontal tail, the fuselage temperatures remained low throughout the entire range of free-stream velocities, except at $q_\infty = 15$ psf for $N/\sqrt{\theta} = 0.87$ where the fuselage temperature reached 400° F. At this point tuft studies showed the reversed-gas flow to be attached to the aft end of the fuselage. Increasing the angle of attack of the airplane from 0° to 4° caused the temperature to decrease to approximately 100°.

Buffet.- The buffet measurements made on the horizontal tail are shown in figure 15. Figure 15(a) shows the variation of the buffet acceleration, $|a/g|$, with the reversed thrust parameter, $-F_G/q_\infty S$, at several values of q_∞.

The results indicate that $|a/g|$ is not only a function of $-F_G/q_\infty S$ but also of q_∞. The most severe buffet accelerations, $|a/g| = 6$, were developed at $q_\infty = 45$ psf where the maximum value of $-F_G/q_\infty S$ was only one-third of the maximum value at $q_\infty = 15$ psf.

Dimensional analysis (see appendix B) of the problem indicated that the dimensionless ratio $(W_t/q_\infty S_t)(|a/g|)$ should be a function of $-F_G/q_\infty S$ and $(EIy)/[q_\infty S_t(l)^3]$, the latter ratio defining the elastic properties of the horizontal tail in bending. The buffet data shown in figure 15(a) are replotted in figure 15(b) in terms of $(W_t/q_\infty S_t)(|a/g|)$ and $-F_G/q_\infty S$, and good correlation is obtained. Thus, it appears that within the limits of these data, the fluctuations in angle of attack and dynamic pressure as well as the mean flow field near the tail are determined by $-F_G/q_\infty S$.

CONCLUDING REMARKS

The full-scale wind-tunnel investigation of a semicylindrical target-type thrust reverser on an F-86D airplane indicated that large nose-down pitching moments were encountered with the reverser in operation. These pitching moments were found to depend on both reversed thrust and forward velocity. Flow surveys showed that these large changes in pitching moment due to the reverser operation were associated with distortion of the flow field near the horizontal tail. Under certain conditions of operation, these distortions increased the angle of attack at the tail sufficiently to stall the horizontal tail.

Generally, it may be stated that the magnitude and direction of the pitching moment due to reverser operation on a single-engine aircraft is dependent on the location of the horizontal tail relative to the reverser.

For the configuration tested, the horizontal tail was above the reversed gases and a pitch-down resulted. If the tail had been below the reversed gases, the flow surveys indicate that a pitch-up would have resulted. Placing the tail high on the vertical fin or relatively far forward would have minimized the change in pitching moment due to reversed thrust.

For this configuration, exhaust gas reingestion was avoided when the free-stream velocity was greater than 15 knots. At high engine power and low airspeed, the temperatures reached a maximum of 500° F on the lower surface of the horizontal tail and 240° F at the rear of the fuselage when the reverser was deflected to 67°. The buffet loads on the horizontal tail increased in severity with increasing reversed thrust and free-stream dynamic pressures.

Within the scope of these tests, the distortion of the flow field due to reverser operation appeared to be a function of the ratio of reversed thrust to the momentum of the free stream.

Ames Research Center
National Aeronautics and Space Administration
Moffett Field, Calif., May 21, 1959

APPENDIX A

DIMENSIONAL ANALYSIS OF THRUST-REVERSER EFFECTS

Assume that the lift on the horizontal tail, L_t, is a function of the tail area, S_t, the distance of the tail ahead of the reverser, x, the distance of the tail above the reverser, z, free-stream velocity, V_∞, free-stream density, ρ_∞, free-stream static pressure, p_∞, reverser jet velocity, V_j, jet density, ρ_j, jet static pressure, p_j, effective angle of the jet from the longitudinal axis, φ_j, and a characteristic length of the reverser, d. Symbolically

$$L_t = f(S_t, x, z, V_\infty, \rho_\infty, p_\infty, V_j, \rho_j, p_j, \varphi_j, d)$$

There are 12 variables in the above relation and three dimensions, force, length, and time. Therefore, there are 12-3 = 9 dimensionless ratios which define the problem. One logical choice would be

$$\frac{L_t}{q_\infty S_t} = C_{L_t} = f\left(\frac{x}{d}, \frac{z}{d}, \frac{q_j}{q_\infty}, \frac{p_\infty}{q_\infty}, \frac{p_j}{q_\infty}, \frac{\rho_j}{\rho_\infty}, \varphi_j, \frac{d^2}{S_t}\right) \tag{A1}$$

In the tests reported herein, it was more convenient to work with reverser gross thrust, rather than directly with any of the above ratios. However, since

$$F_G = (\rho_j V_j^2 + p_j - p_\infty) A_j \cos \varphi_j \tag{A2}$$

or

$$\frac{F_G}{q_\infty A_j} = \left(\frac{2q_j}{q_\infty} + \frac{p_j}{q_\infty} - \frac{p_\infty}{q_\infty}\right)\cos \varphi_j$$

the ratio q_j/q_∞ can be expressed as a function of $F_G/q_j d^2$, p_j/q_∞, p_∞/q_∞, and φ. Therefore, equation (A1) can be written

$$C_{L_t} = g\left(\frac{x}{d}, \frac{z}{d}, \frac{F_G}{q_\infty d^2}, \frac{p_\infty}{q_\infty}, \frac{p_j}{q_\infty}, \frac{\rho_j}{\rho_\infty}, \varphi_j, \frac{d^2}{S_t}\right) \tag{A3}$$

For convenience, the ratio $F_G/q_\infty d^2$ may be replaced by $F_G/q_\infty S$, thus putting it in the conventional form for thrust coefficient. Equation (A3) may then be written

$$C_{L_t} = h\left(\frac{x}{d}, \frac{z}{d}, \frac{F_G}{q_\infty S}, \frac{p_\infty}{q_\infty}, \frac{p_j}{q_\infty}, \frac{\rho_j}{\rho_\infty}, \varphi_j, \frac{d^2}{S}, \frac{S_t}{S}\right) \tag{A4}$$

For the range of variables covered in these tests, the ratios p_∞/q_∞, p_j/q_∞, and ρ_j/ρ_∞ appear to be of secondary importance, and possibly may not need to be duplicated in model tests to obtain meaningful results. Thus, equation (A4) could be approximated by

$$C_{L_t} \approx h\left(\frac{x}{d}, \frac{z}{d}, \varphi_j, \frac{d^2}{S}, \frac{S_t}{S}, \frac{F_G}{q_\infty S}\right)$$

in which $F_G/q_\infty S$ is the only operating condition to be simulated and the rest of the ratios are determined by the condition of geometric similarity.

APPENDIX B

ANALYSIS OF HORIZONTAL TAIL BUFFET

If it is assumed that the motion of the tip of the horizontal tail can be approximated by a simple one degree of freedom system, then

$$\frac{W_t}{g}\frac{d^2y}{dt^2} = L_t - ky \tag{B1}$$

where

y deflection of the tip of the horizontal tail

W_t weight of the horizontal tail

k stiffness of the horizontal tail on bending

L_t lift on horizontal tail, $C_{L_{\alpha_t}}(\alpha_t)(q_t)(S_t)$

$C_{L_{\alpha_t}}$ lift curve slope of horizontal tail

Assume that

$$q_t = q_\infty + \Delta q = q_\infty\left(1 + \frac{\Delta q}{q_\infty}\right)$$

Further assume that for a given reverser setting

$$1 + \frac{\Delta q}{q_\infty} = f\left(\frac{F_G}{q_\infty S}\right) \tag{B2}$$

and

$$\alpha_t = g\left(\frac{F_G}{q_\infty S}\right) \tag{B3}$$

then

$$\left.\begin{aligned} L_t &= C_{L_{\alpha_t}} q_\infty S_t f\left(\frac{F_G}{q_\infty S}\right) g\left(\frac{F_G}{q_\infty S}\right) \\ L_t &= C_{L_{\alpha_t}} q_\infty S_t h\left(\frac{F_G}{q_\infty S}\right) \end{aligned}\right\} \tag{B4}$$

The stiffness, k, can be written as

$$k = \frac{y_{static}}{F_{static}} = \frac{CEI}{l^3} \tag{B5}$$

where

y_{static} deflection due to static force, F_{static}

E modulus of elasticity

I moment of inertia

l horizontal tail semispan

C dimensionless constant

Substituting equations (B4) and (B5) in equation (B1) gives

$$\frac{W_t}{g}\frac{d^2y}{dt^2} + \frac{CEI}{l^3}y = C_{L\alpha_t} q_\infty S_t h\left(\frac{F_G}{q_\infty S}\right)$$

or with $d^2y/dt^2 = a$

$$\frac{W_t}{q_\infty S_t}\left(\left|\frac{a}{g}\right|\right) = C_{L\alpha_t} h\left(\frac{F_G}{q_\infty S}\right) - \frac{CEI}{q_\infty S_t l^2}\frac{y}{l} \tag{B6}$$

The correlation of $(W_t/q_\infty S_t)(|a/g|)$ with $F_G/q_\infty S$ shown in figure 15(b) of this report indicates that the assumption that the fluctuations of q_t and α_t are determined by $F_G/q_\infty S$ (represented by eqs. (B2) and (B3)) is valid for the conditions covered in these tests.

REFERENCES

1. Anderson, Seth B., Cooper, George E., and Faye, Alan E., Jr: Flight Measurements of the Effect of a Controllable Thrust Reverser on the Flight Characteristics of a Single-Engine Jet Airplane. NASA MEMO 4-26-59A, 1959.

2. Tolhurst, William H., Jr.: Downwash Characteristics and Vortex-Sheet Shape Behind a 63° Swept-Back Wing-Fuselage Combination at a Reynolds Number of 6.1×10^{6}. NACA TN 3175, 1954.

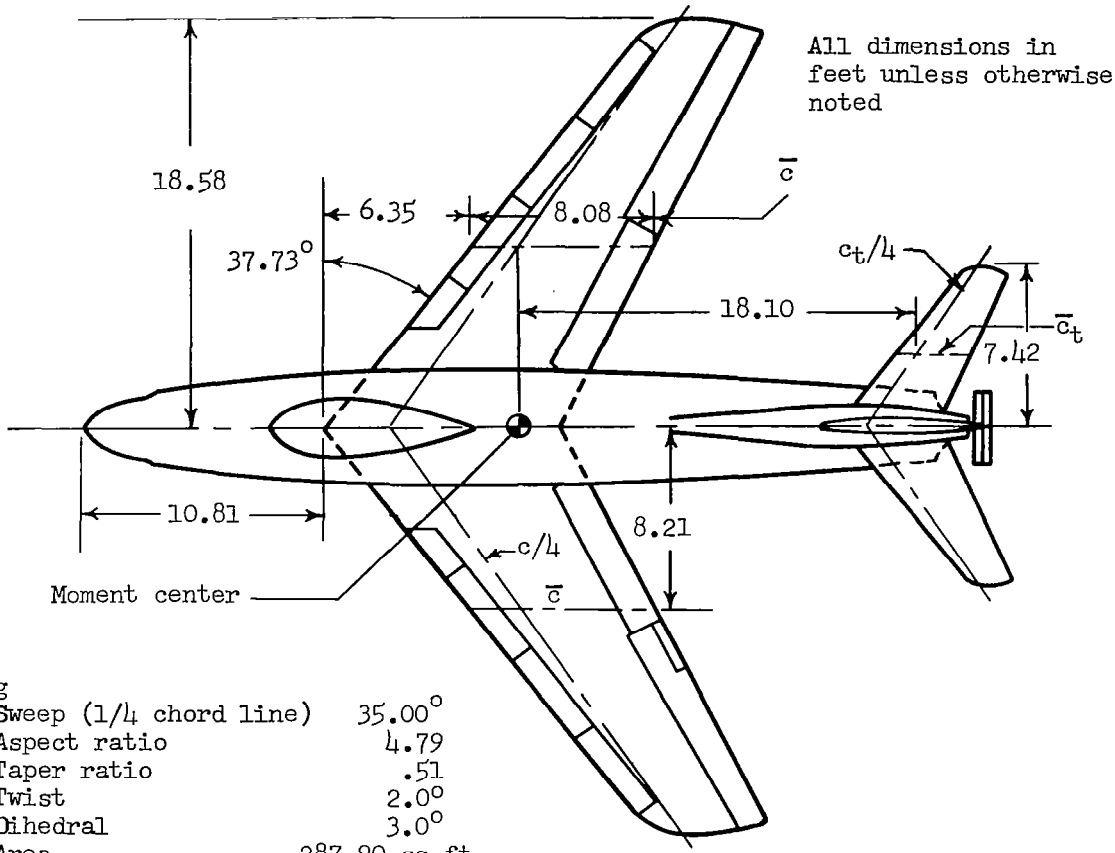

Wing

Sweep (1/4 chord line)	35.00°
Aspect ratio	4.79
Taper ratio	.51
Twist	2.0°
Dihedral	3.0°
Area	287.90 sq ft

Horizontal tail

Sweep	35.00°
Aspect ratio	4.73
Taper ratio	.451
Twist	0°
Dihedral	0°
Area	46.5 sq ft

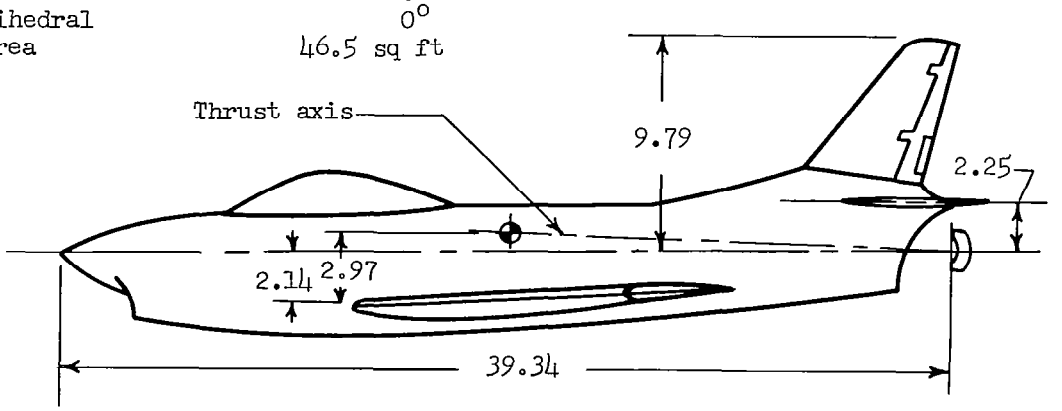

Figure 1.- General arrangement of the YF-86D airplane.

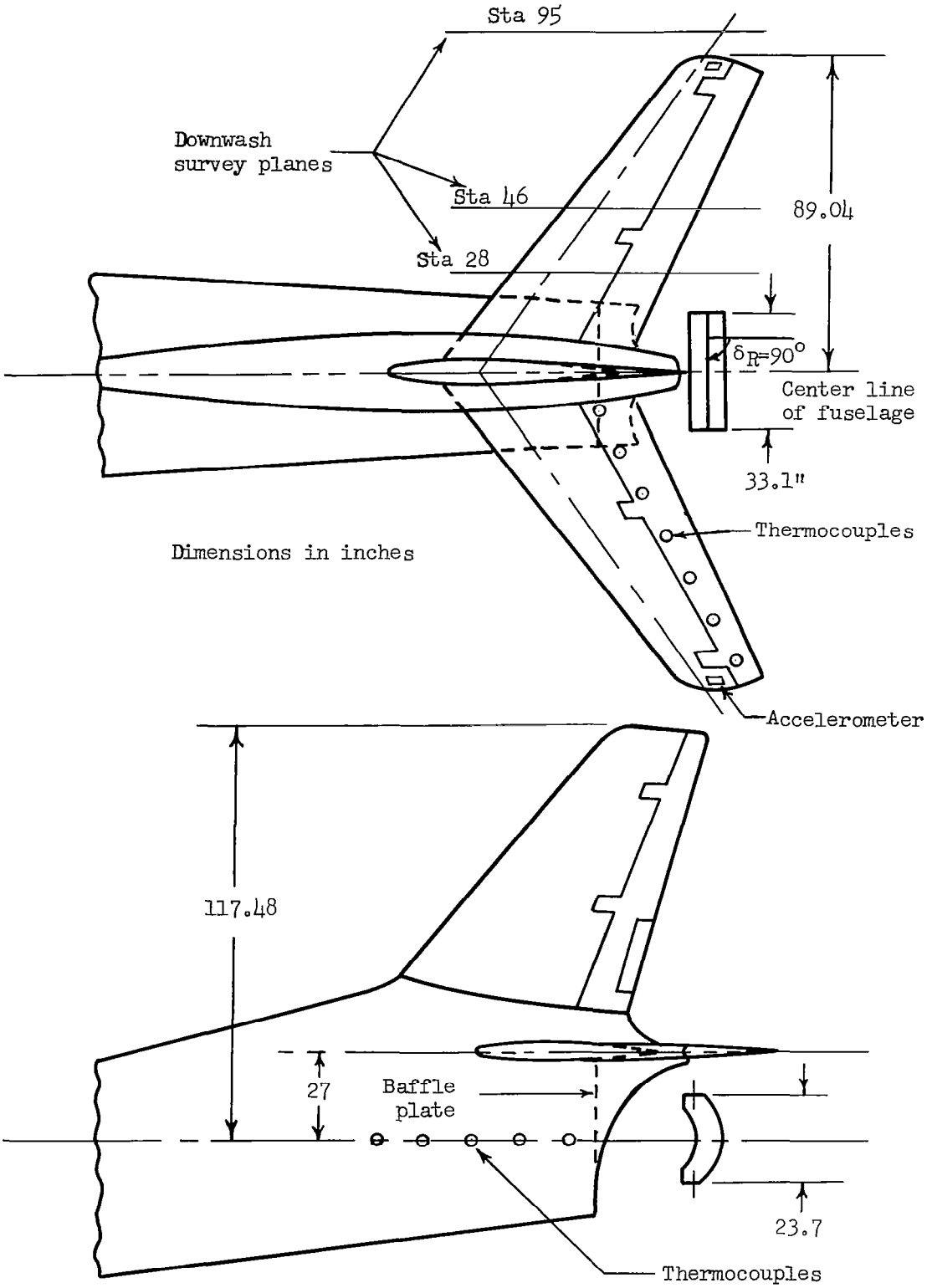

(a) Location of the thrust reverser relative to the rear of the fuselage.

Figure 2.- Details of the thrust-reverser installation.

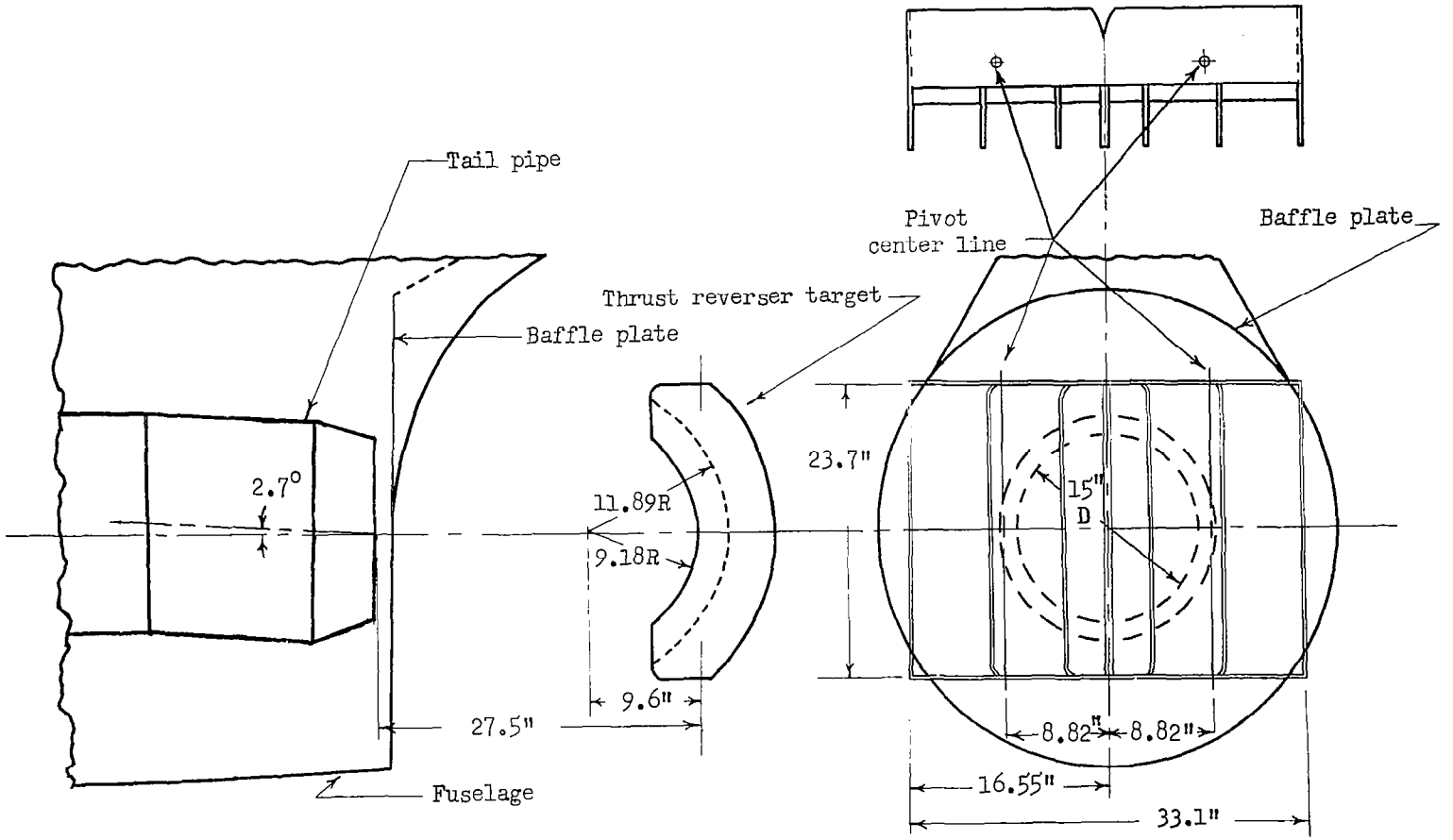

(b) Details of reverser construction.

Figure 2.- Continued.

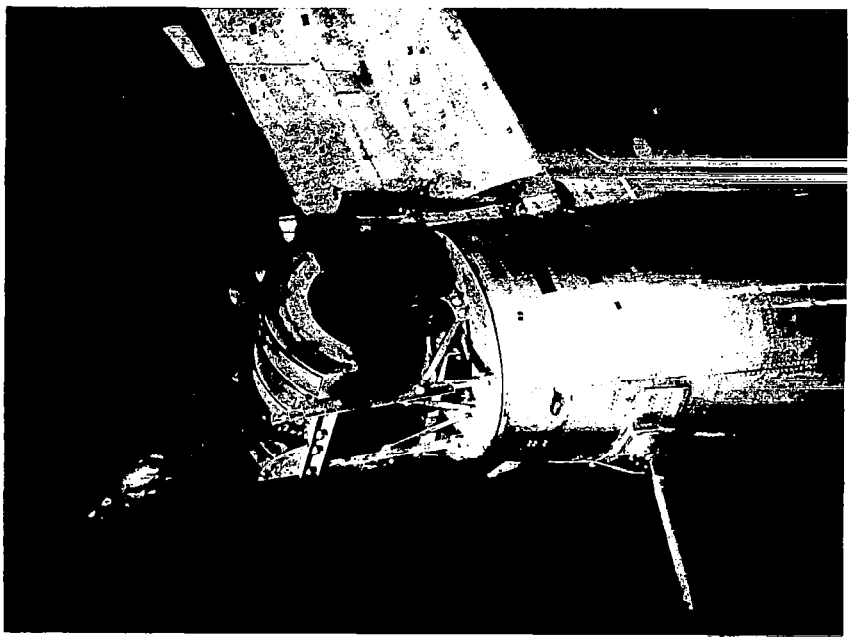

A-22929

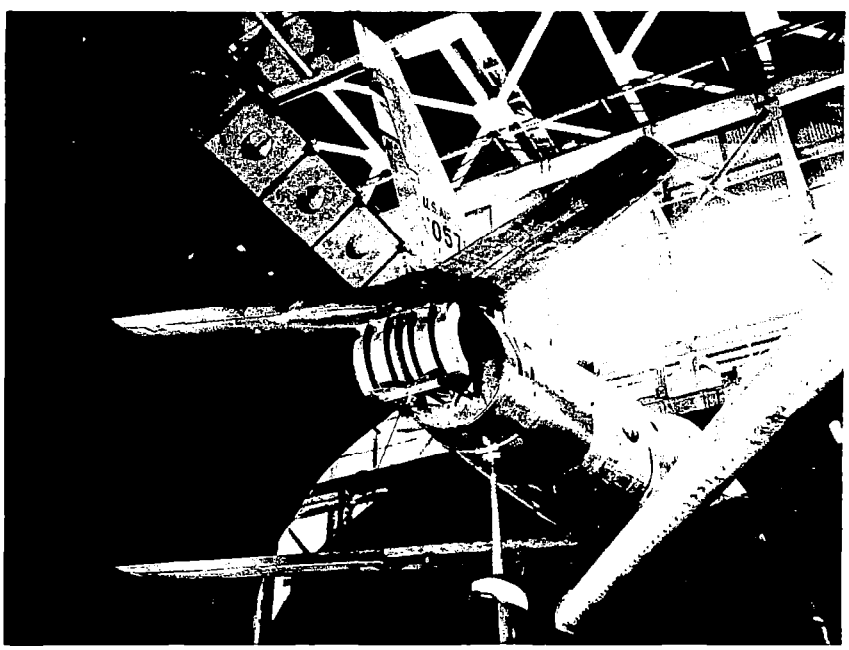

A-22930

(c) Photographs of the reverser installation on the airplane.

Figure 2.- Concluded.

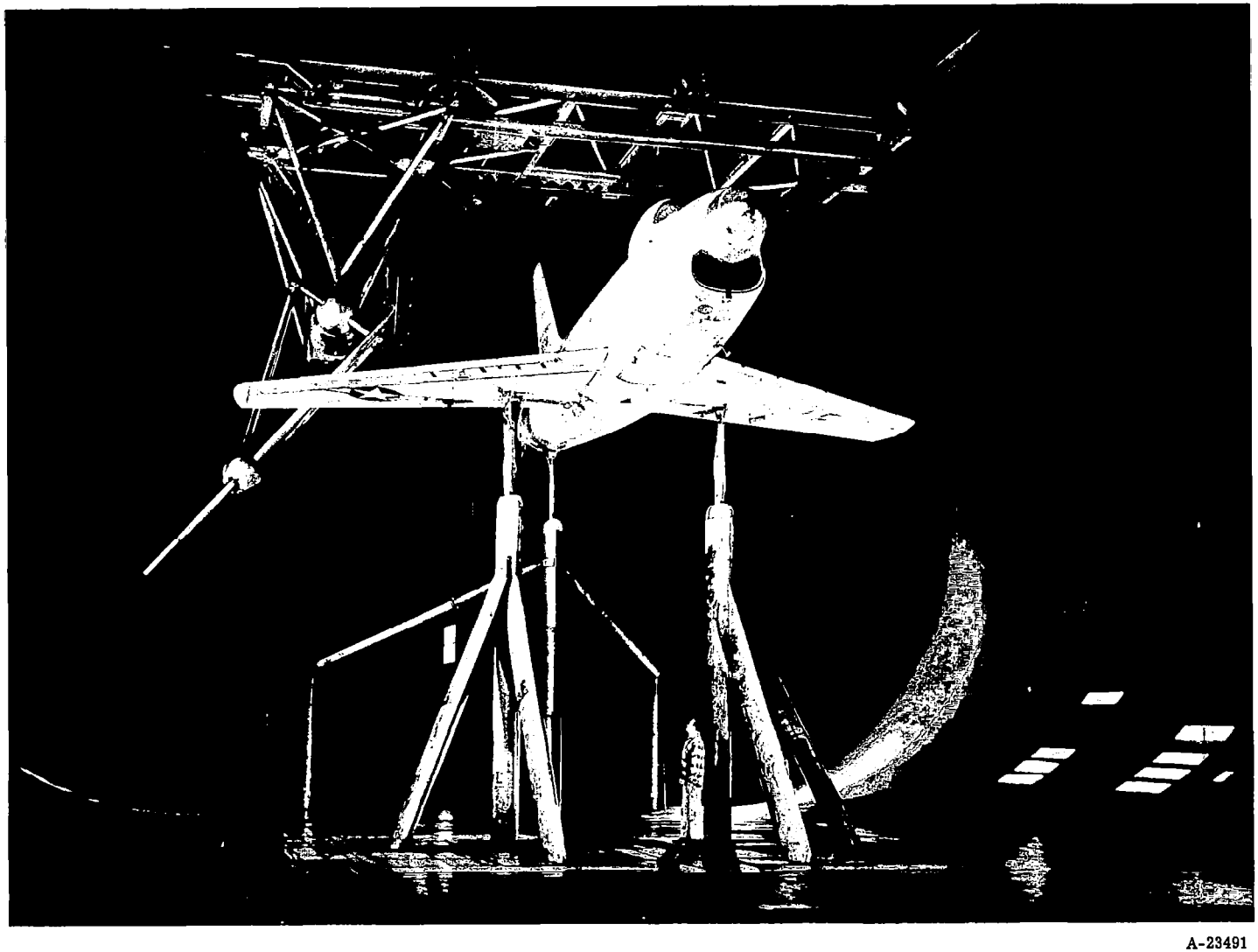

A-23491

Figure 3.- Photograph of the YF-86D airplane and survey apparatus in the Ames 40- by 80-foot wind tunnel.

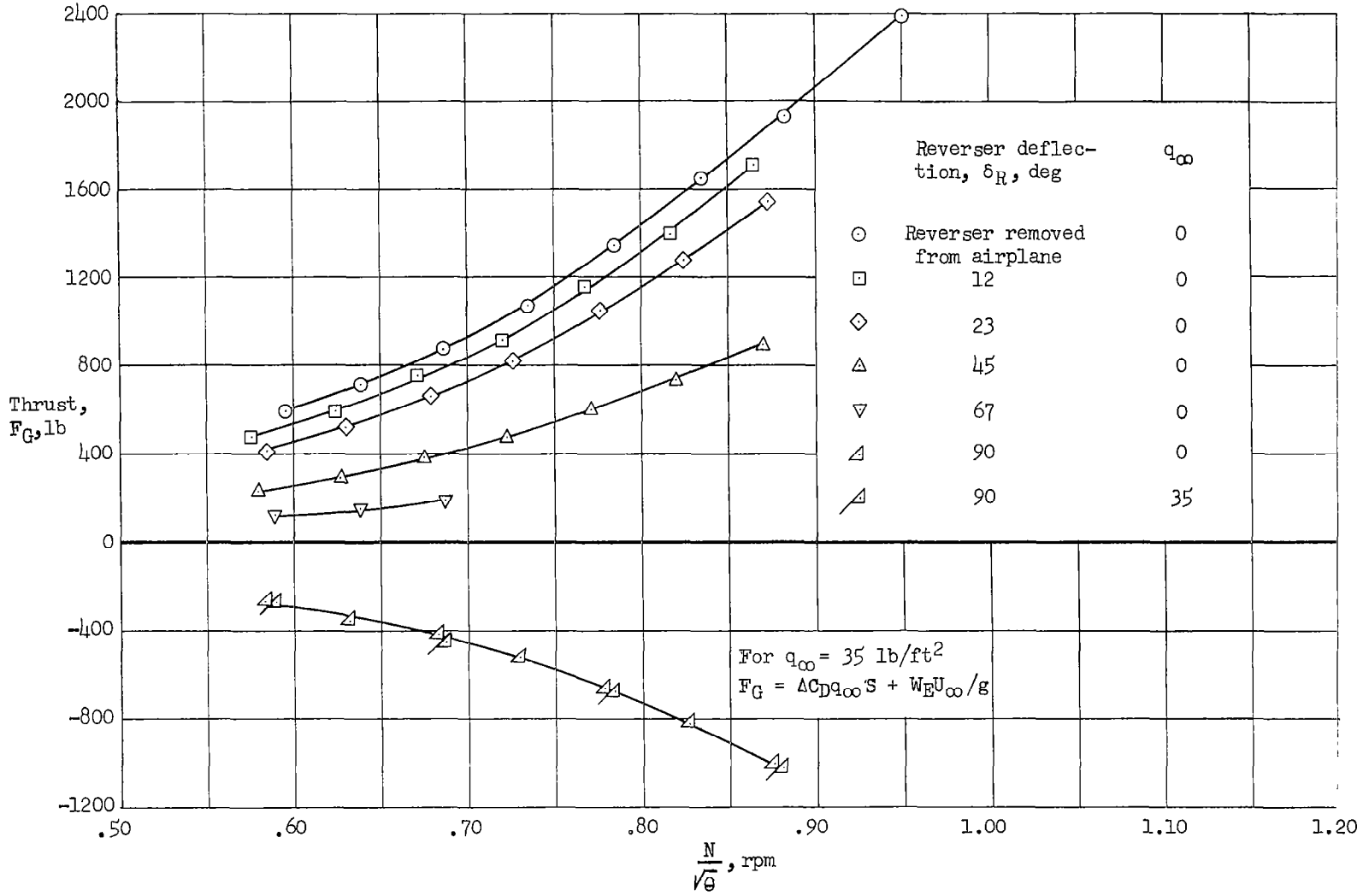

Figure 4.- Variation of gross thrust with changes in corrected engine speed for various reverser deflection angles, tail on.

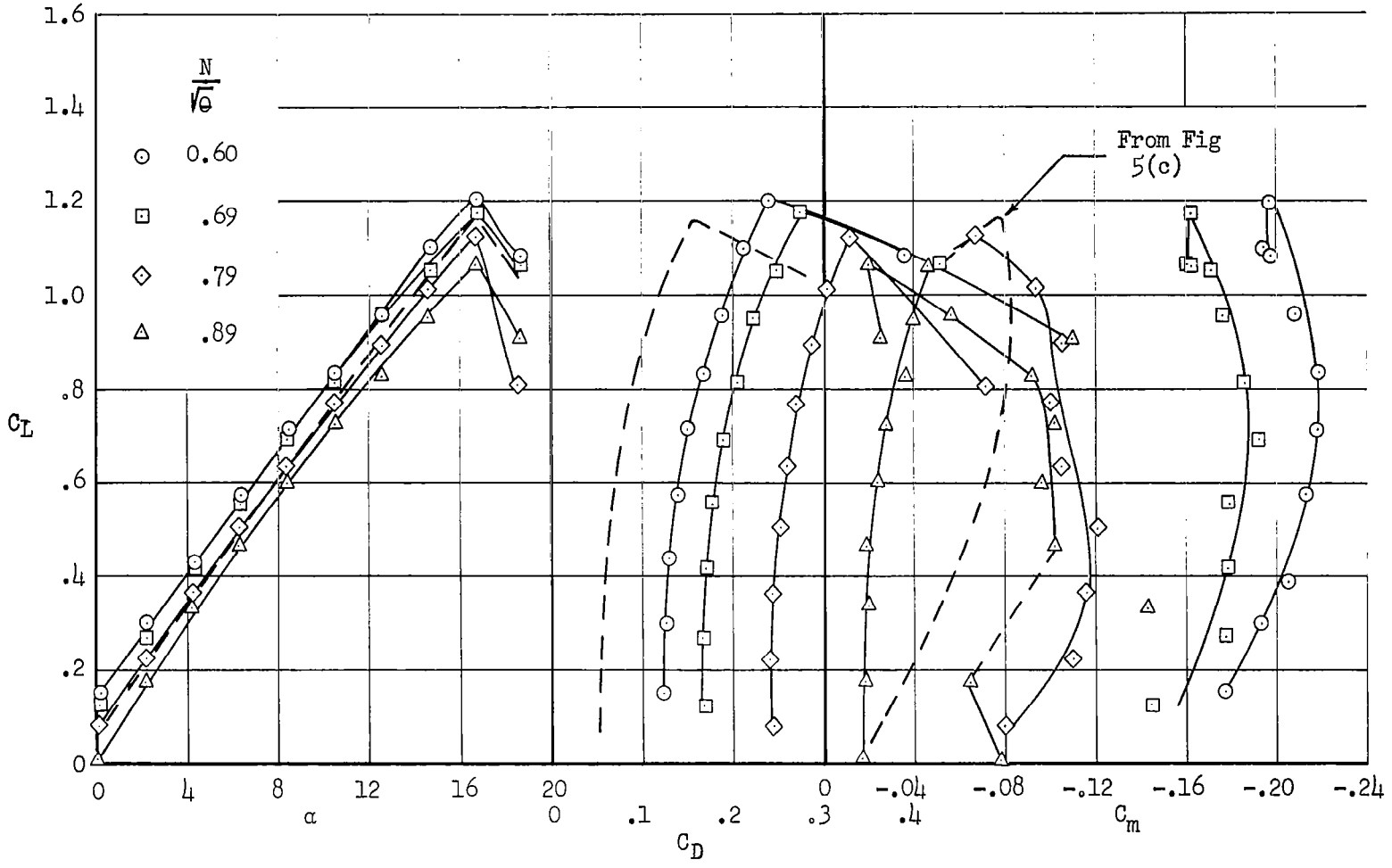

(a) q_∞ = 15 psf

Figure 5.- The effect of thrust reversal on the longitudinal characteristics of the airplane at various free-stream dynamic pressures and engine speeds; $\delta_R = 90^\circ$, $i_t = 0^\circ$.

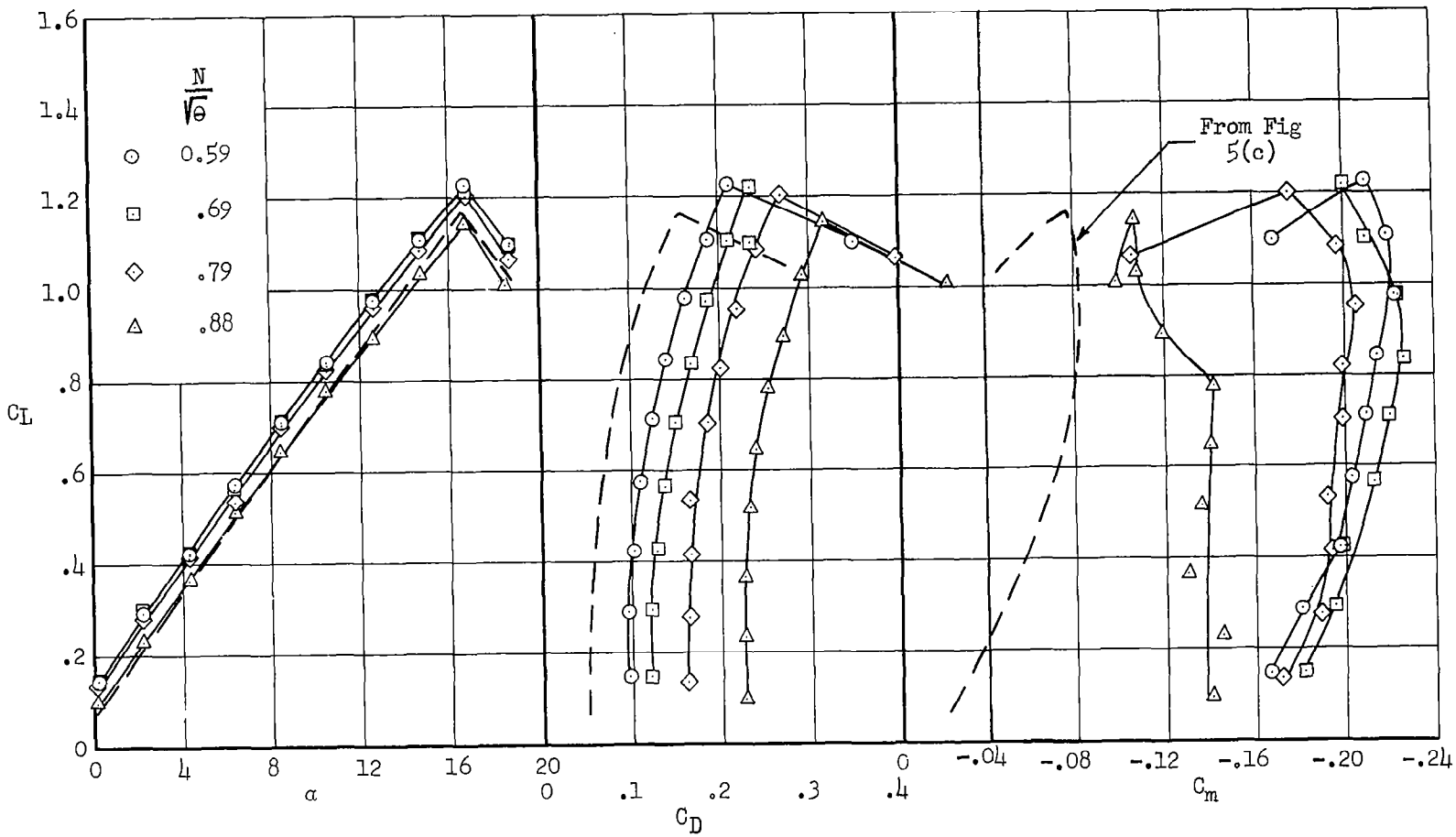

(b) q_∞ = 25 psf

Figure 5.- Continued.

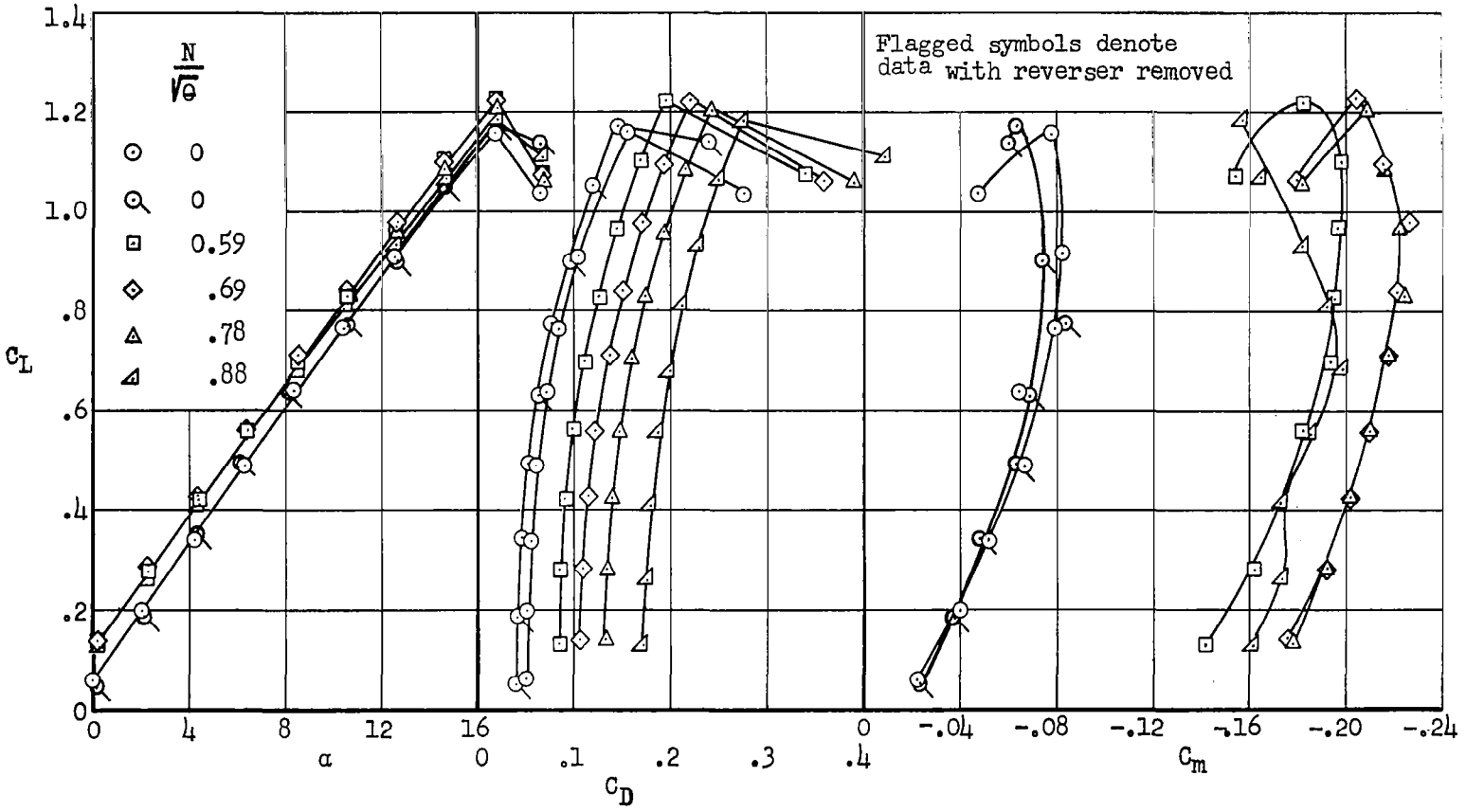

(c) q_∞ = 35 psf

Figure 5.- Continued.

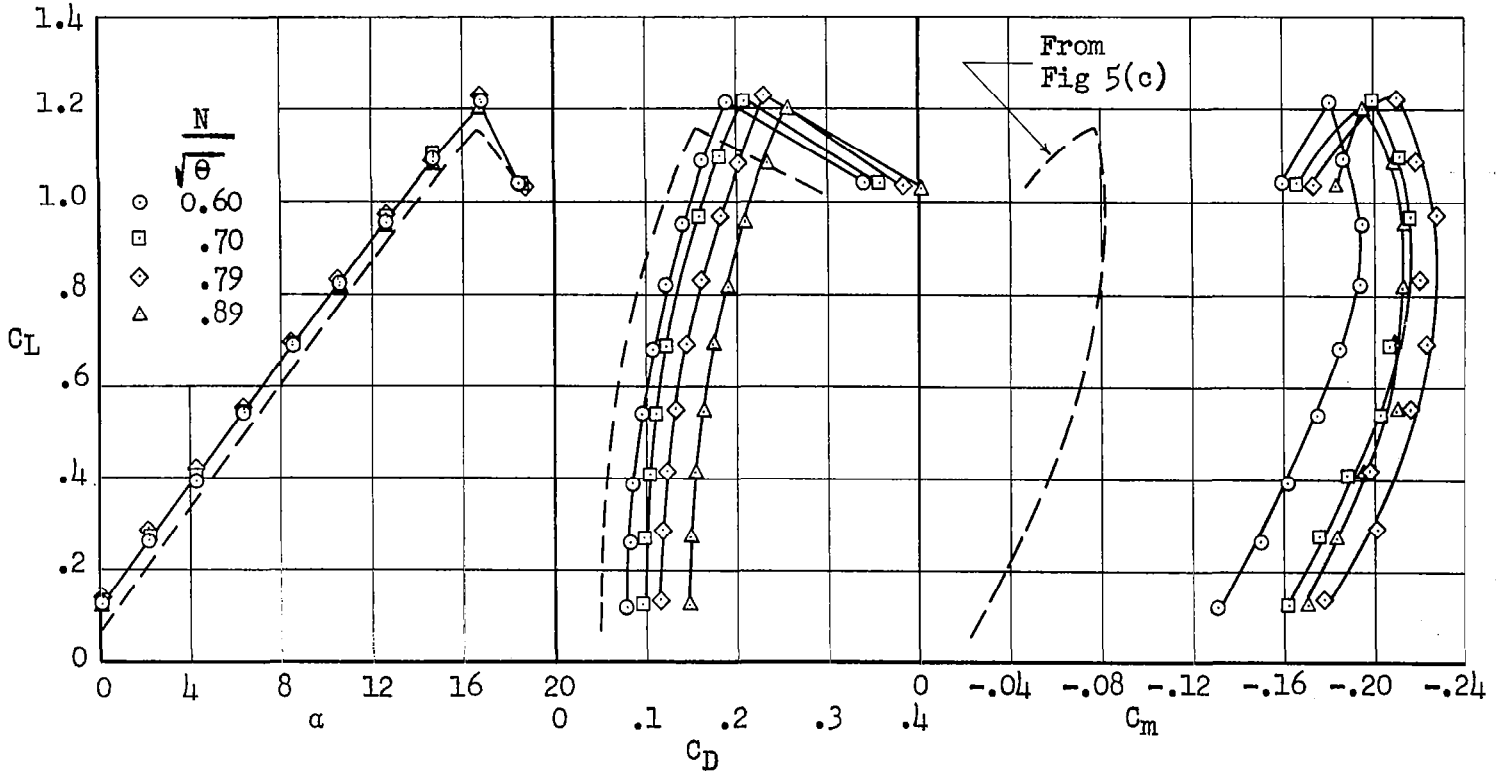

(d) q_∞ = 45 psf

Figure 5.- Concluded.

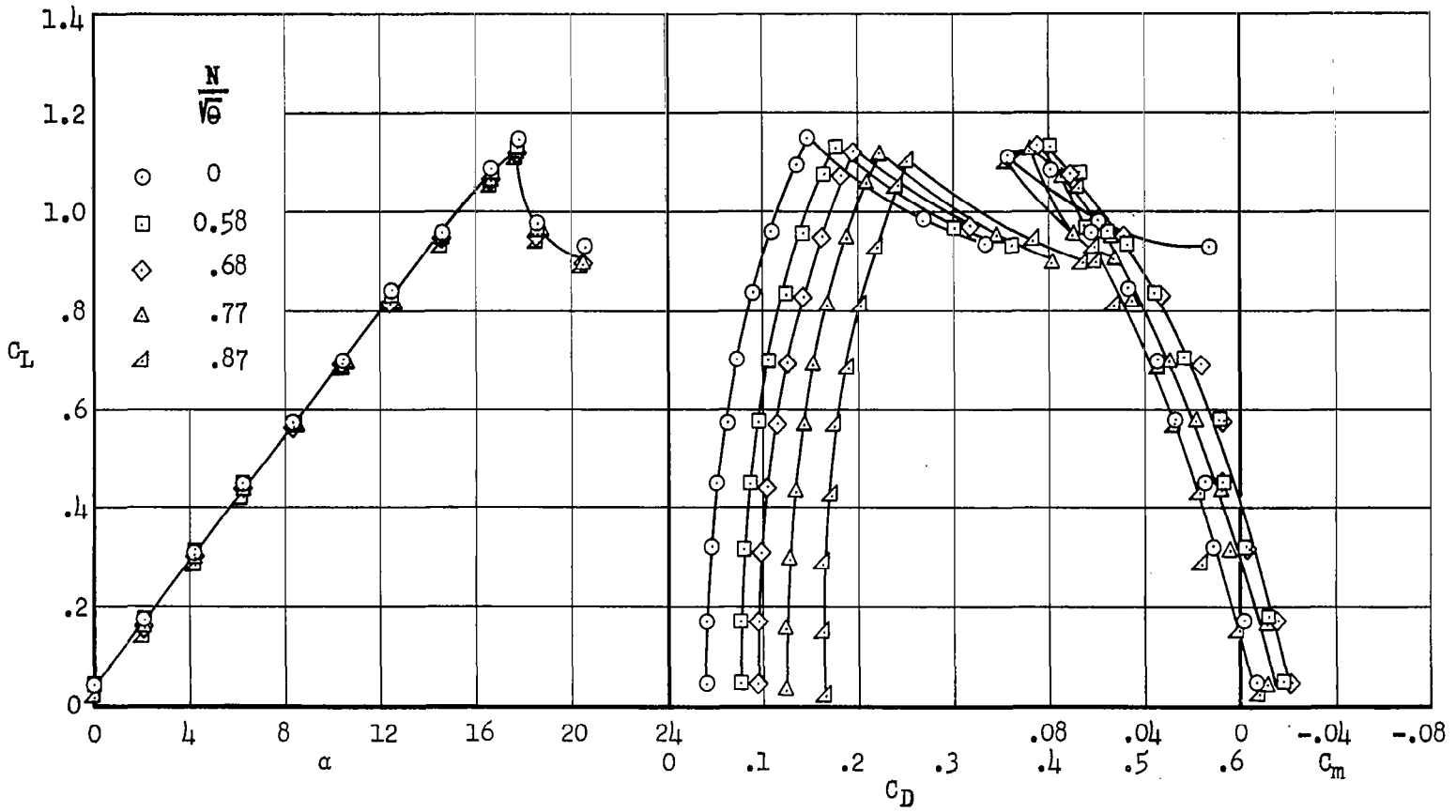

Figure 6.- The effect of thrust reversal on the longitudinal characteristics of the airplane; q_∞ = 35 psf, δ_R = 90°, horizontal tail off.

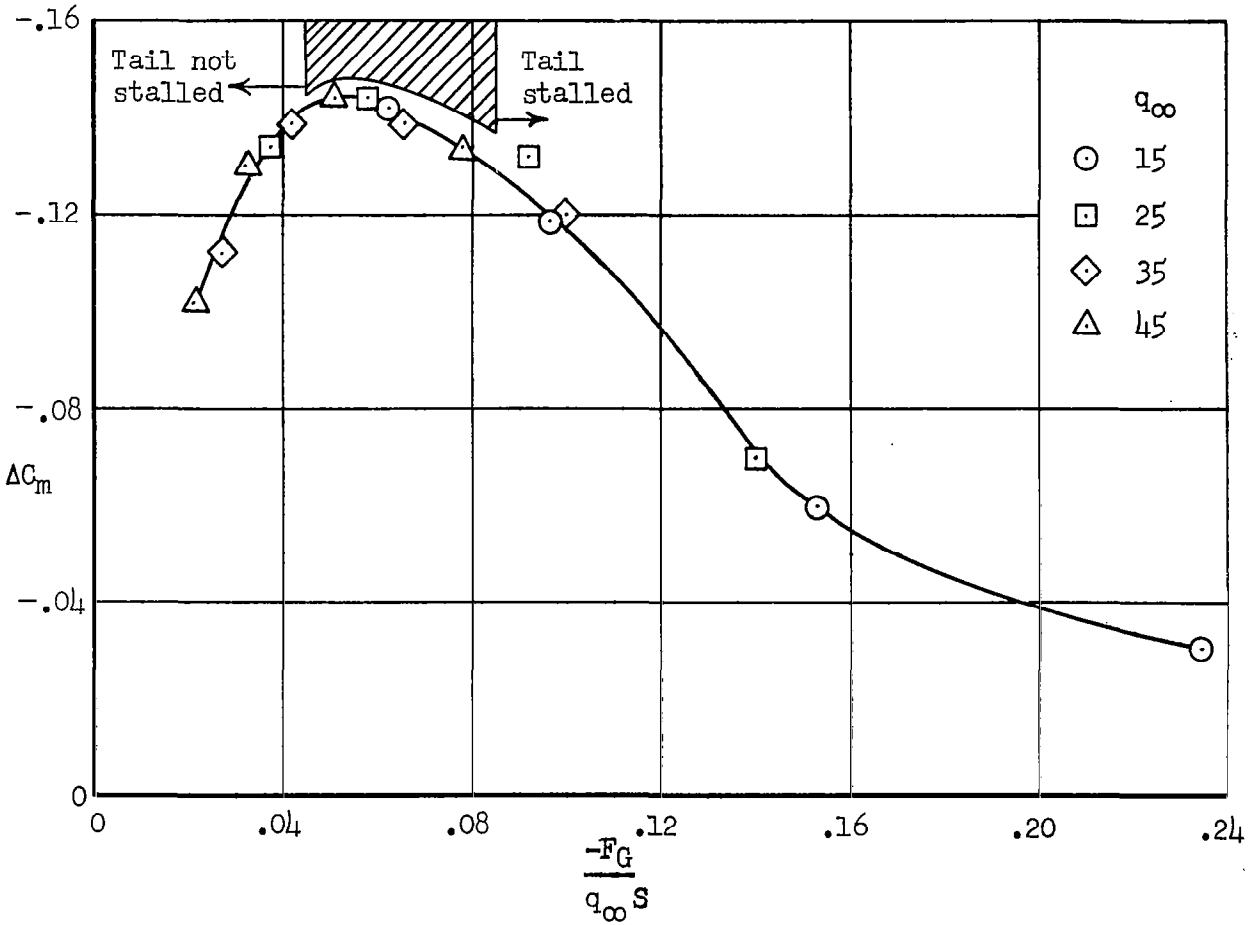

Figure 7.- Variation of ΔC_m due to reversed thrust with change in the reversed thrust parameter $-F_G/q_\infty S$; $\delta_R = 90^\circ$, $C_L = 0.4$.

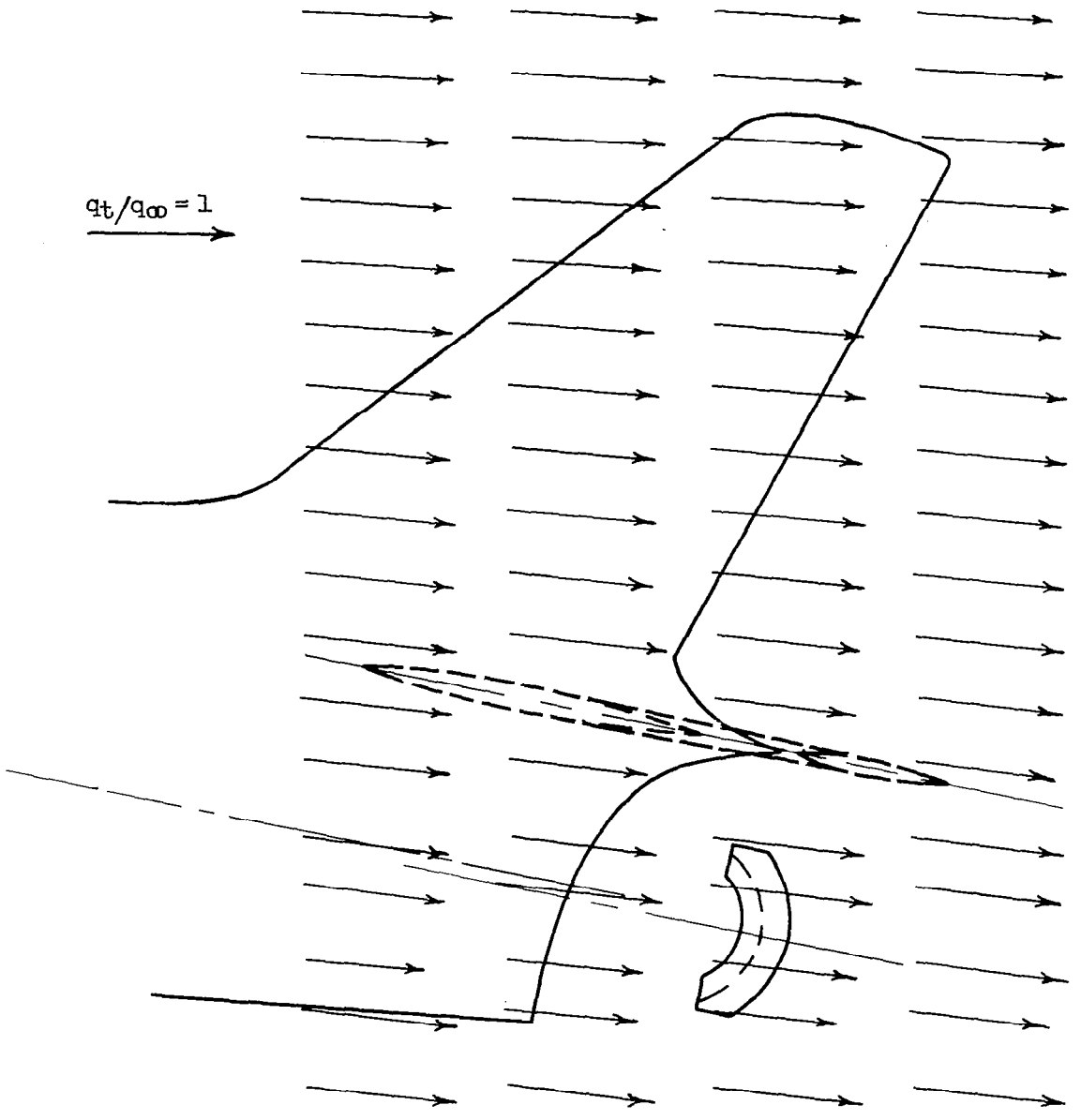

Figure 8.- The flow field around the rear of the fuselage, station 95, typical of all spanwise stations; $-F_G/q_\infty S = 0$, $q_\infty = 35$ psf; $\alpha = 11.2^\circ$.

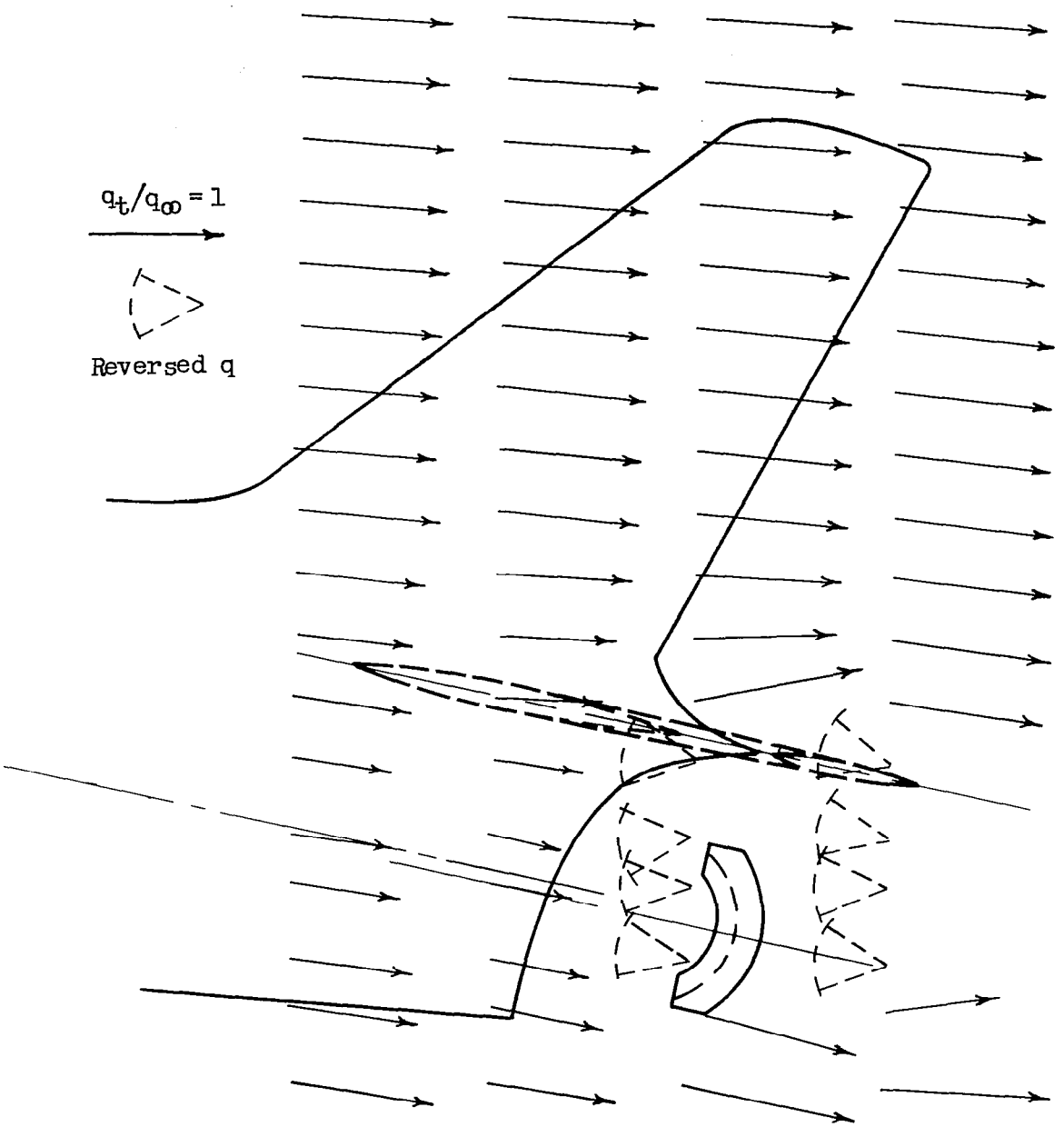

(a) Station 28.

Figure 9.- The flow field around the rear of the fuselage; $-F_G/q_\infty S = 0.03$, $q_\infty = 35$ psf, $\alpha = 11.2^\circ$.

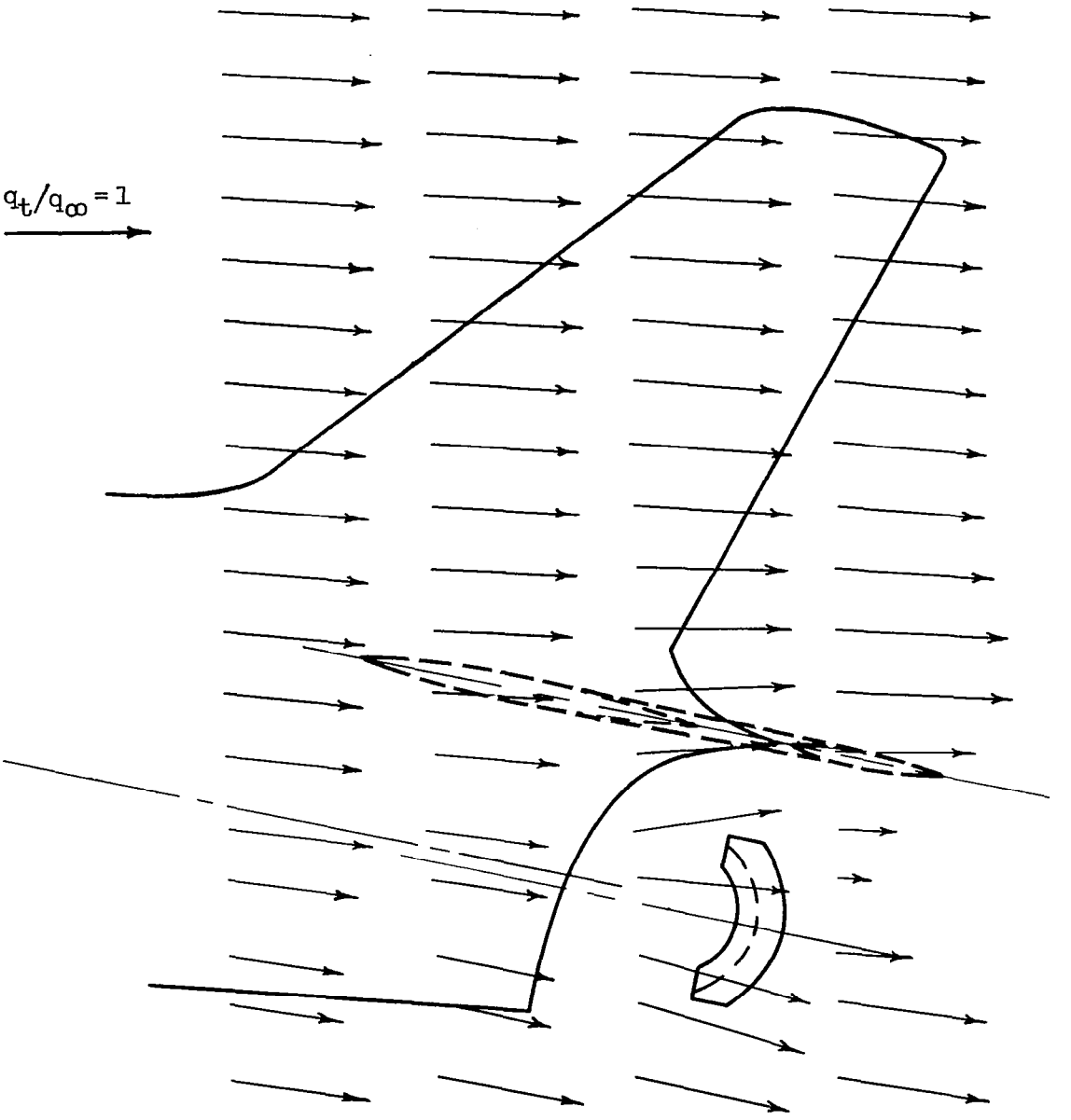

(b) Station 46.

Figure 9.- Continued.

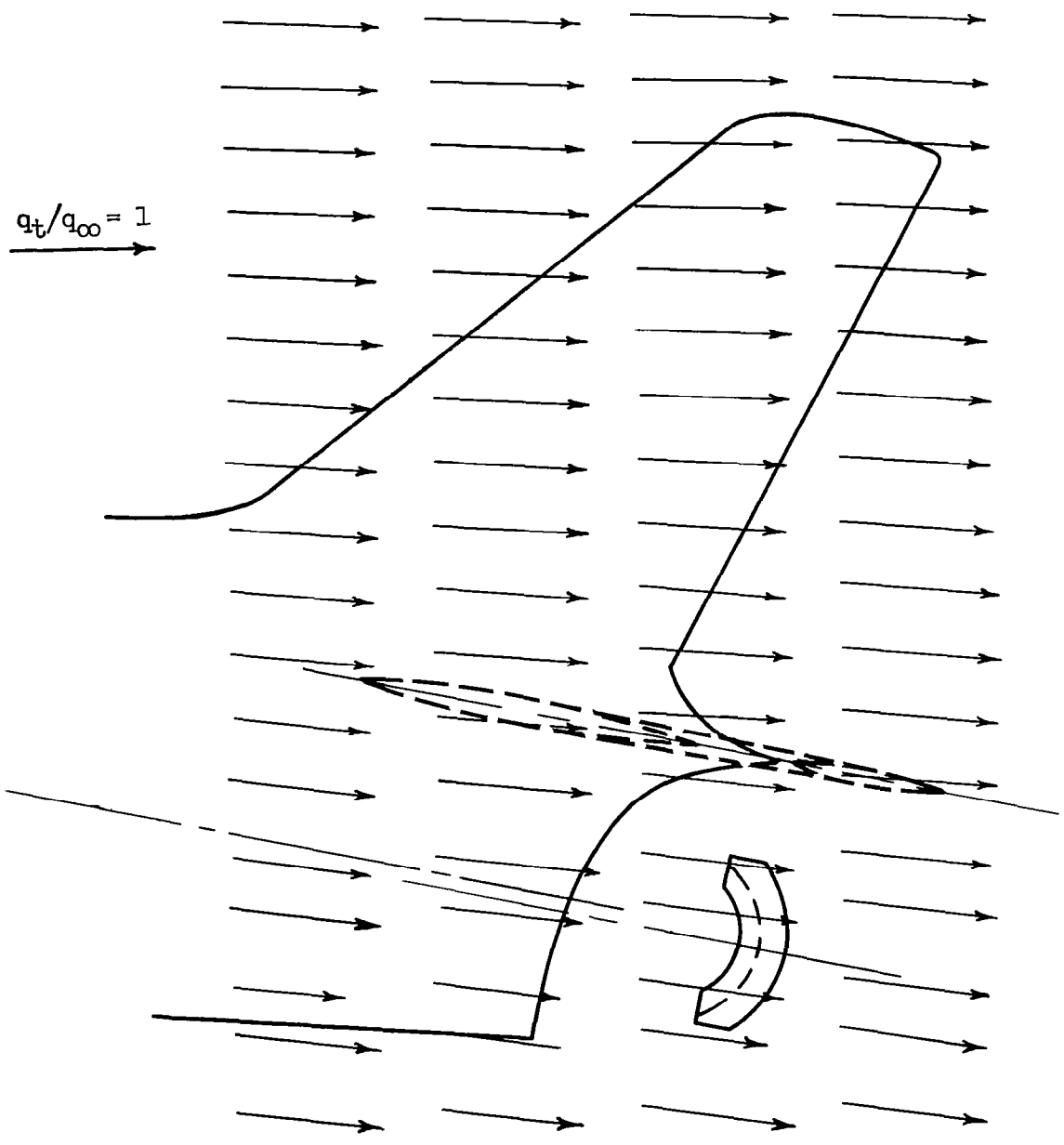

(c) Station 95.

Figure 9.- Concluded.

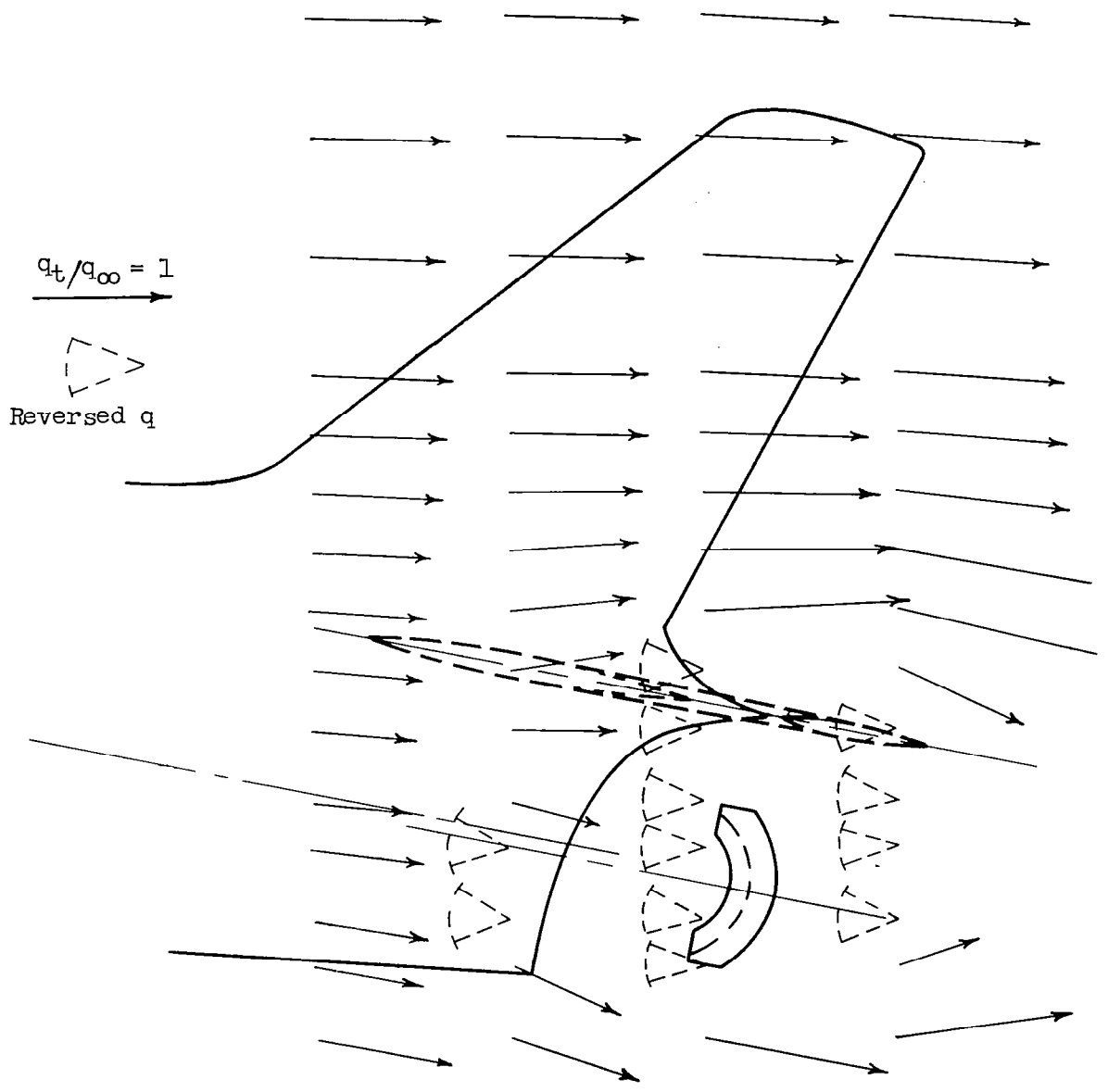

(a) Station 28.

Figure 10.- The flow field around the rear of the fuselage; $-F_G/q_\infty S = 0.10$, $q_\infty = 35$ psf, $\alpha = 11.2^\circ$.

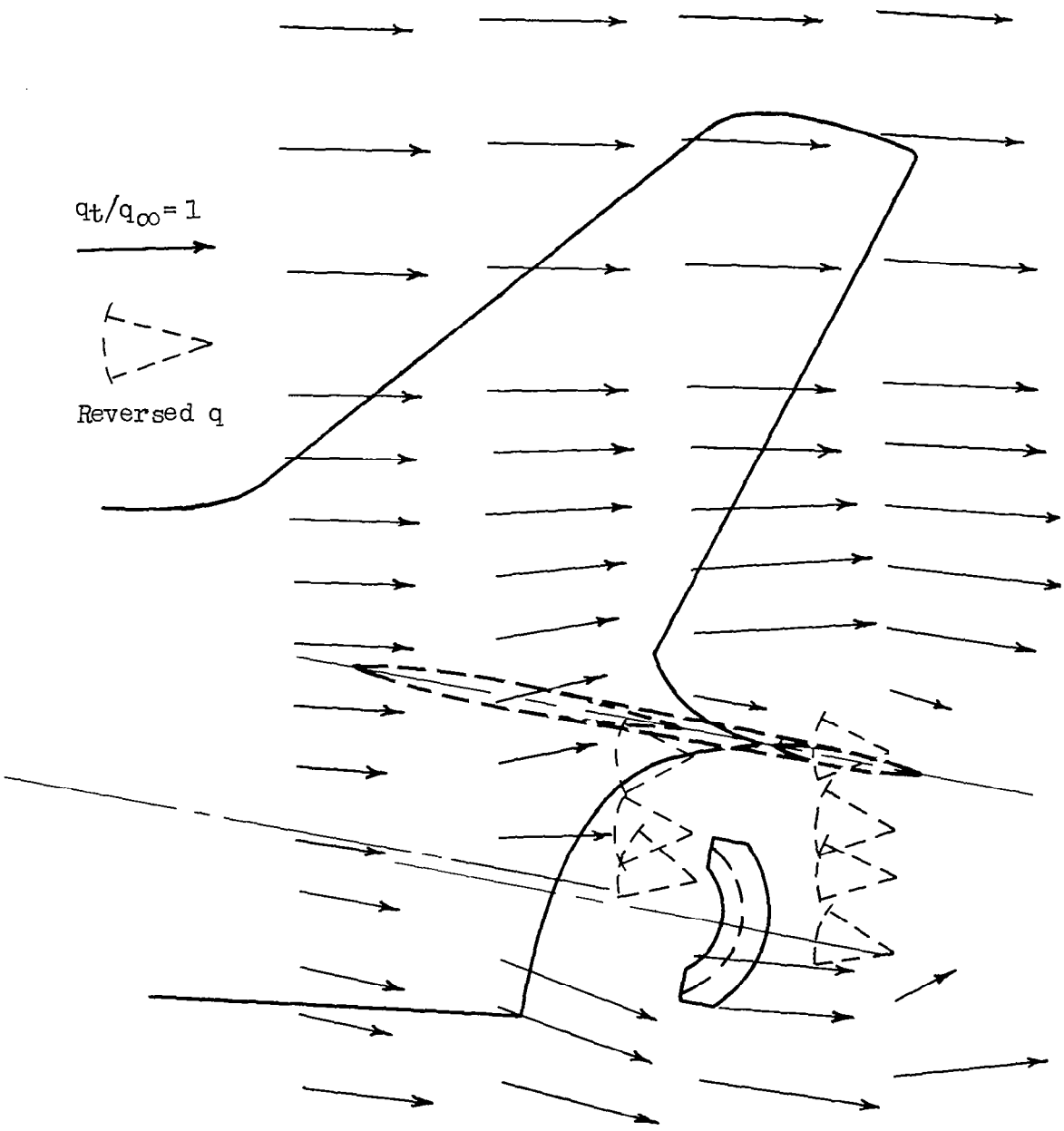

(b) Station 46.

Figure 10.- Continued

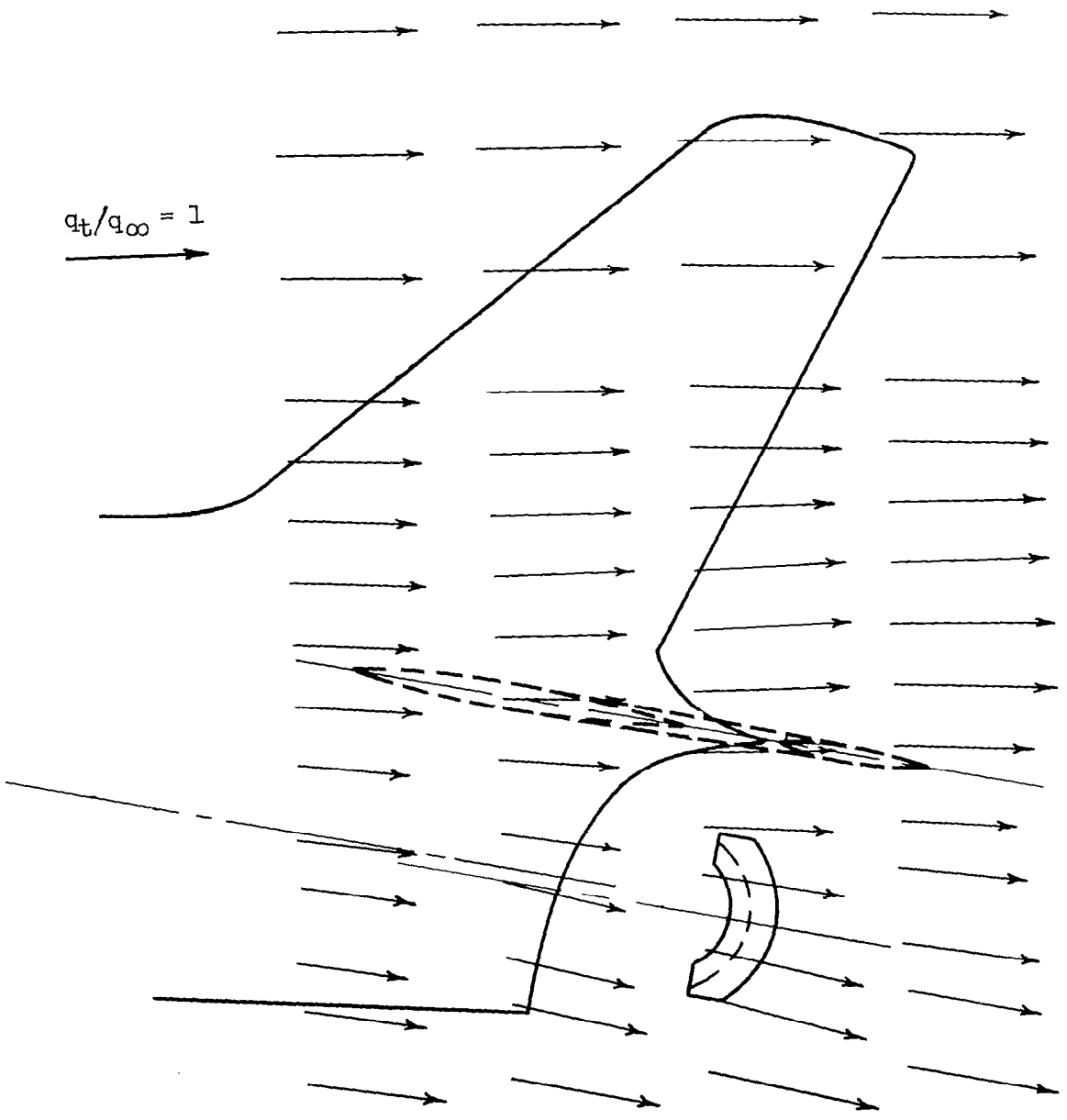

(c) Station 95.

Figure 10.- Concluded.

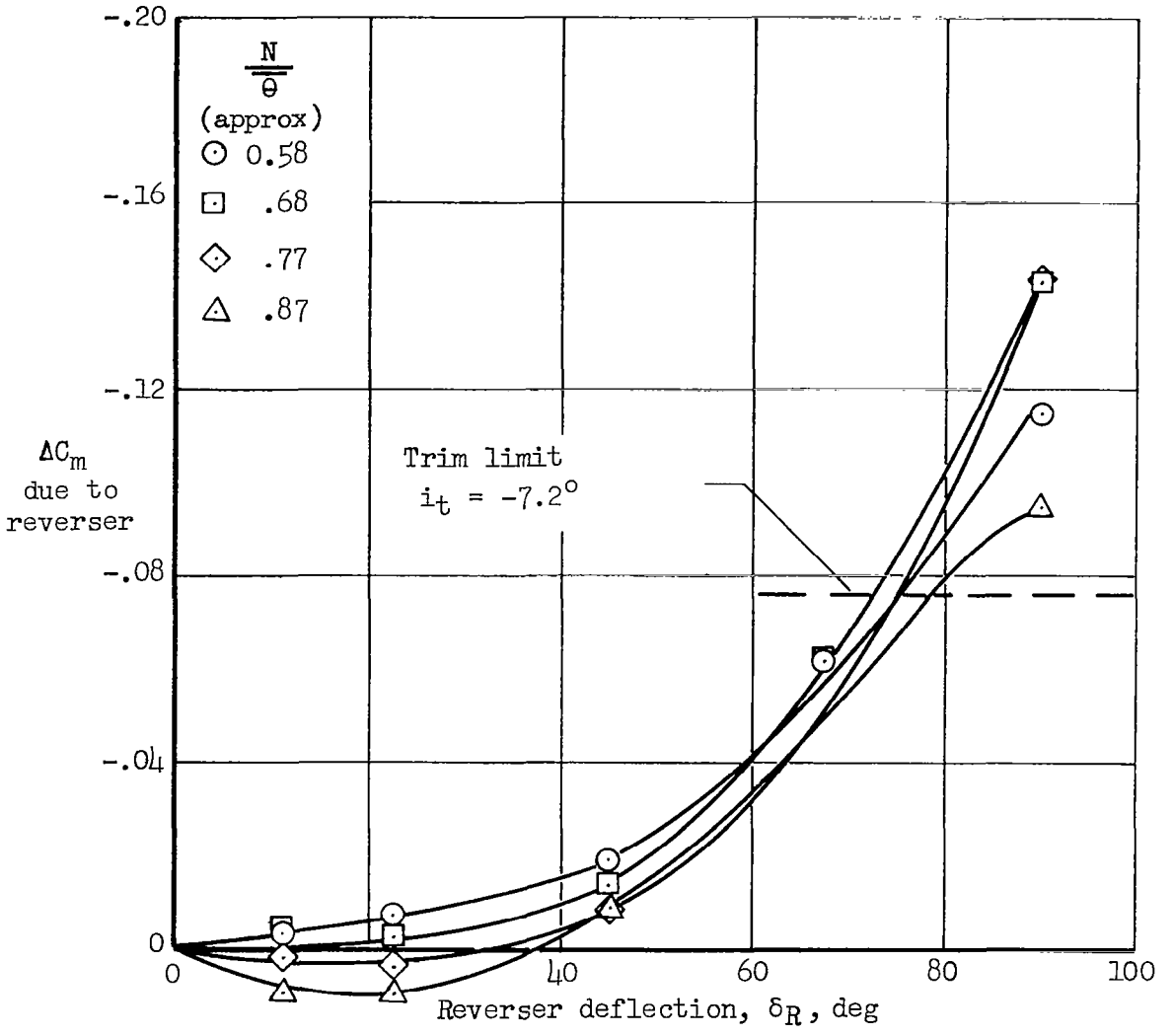

Figure 11.- The variation of ΔC_m due to reversed thrust with change in the reverser deflection angle; q_∞ = 35 psf, C_L = 0.4, horizontal tail on.

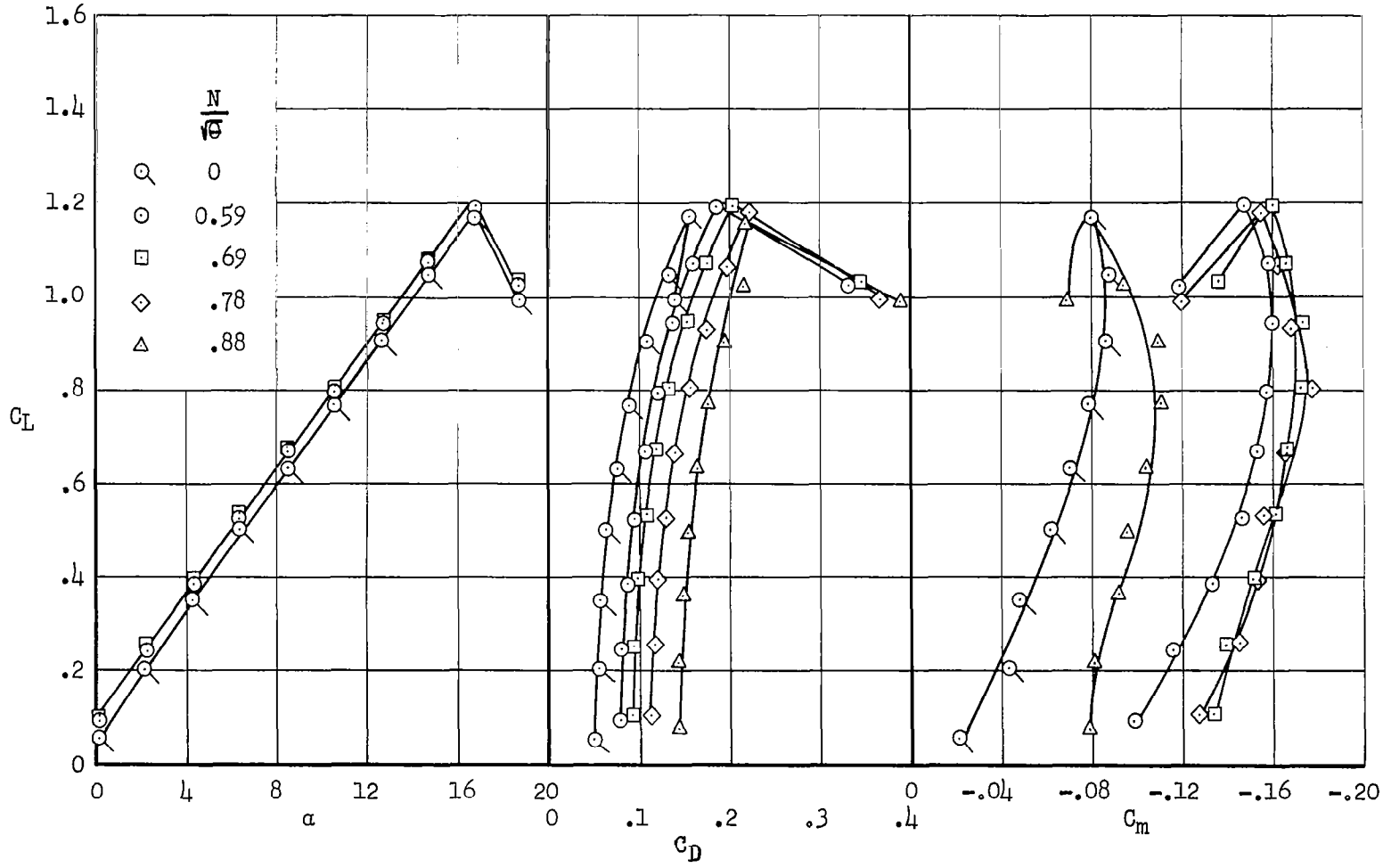

(a) Target tilted up 10°.

Figure 12.- The effect of reverser target tilt on the longitudinal characteristics of the airplane; $\delta_R = 90°$, $q_\infty = 45$ psf, $i_t = 0°$.

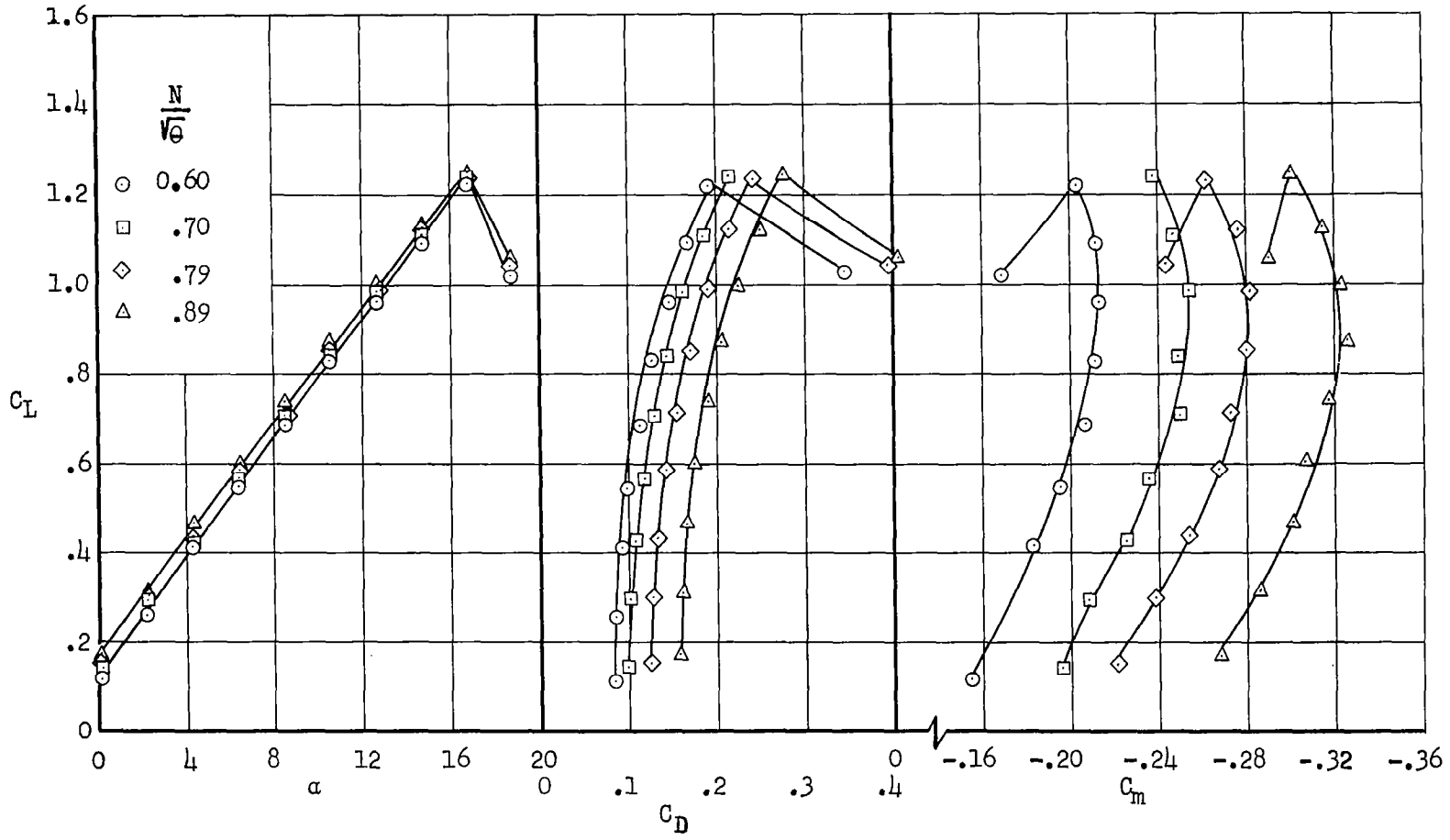

(b) Target tilted down 10°.

Figure 12.- Concluded.

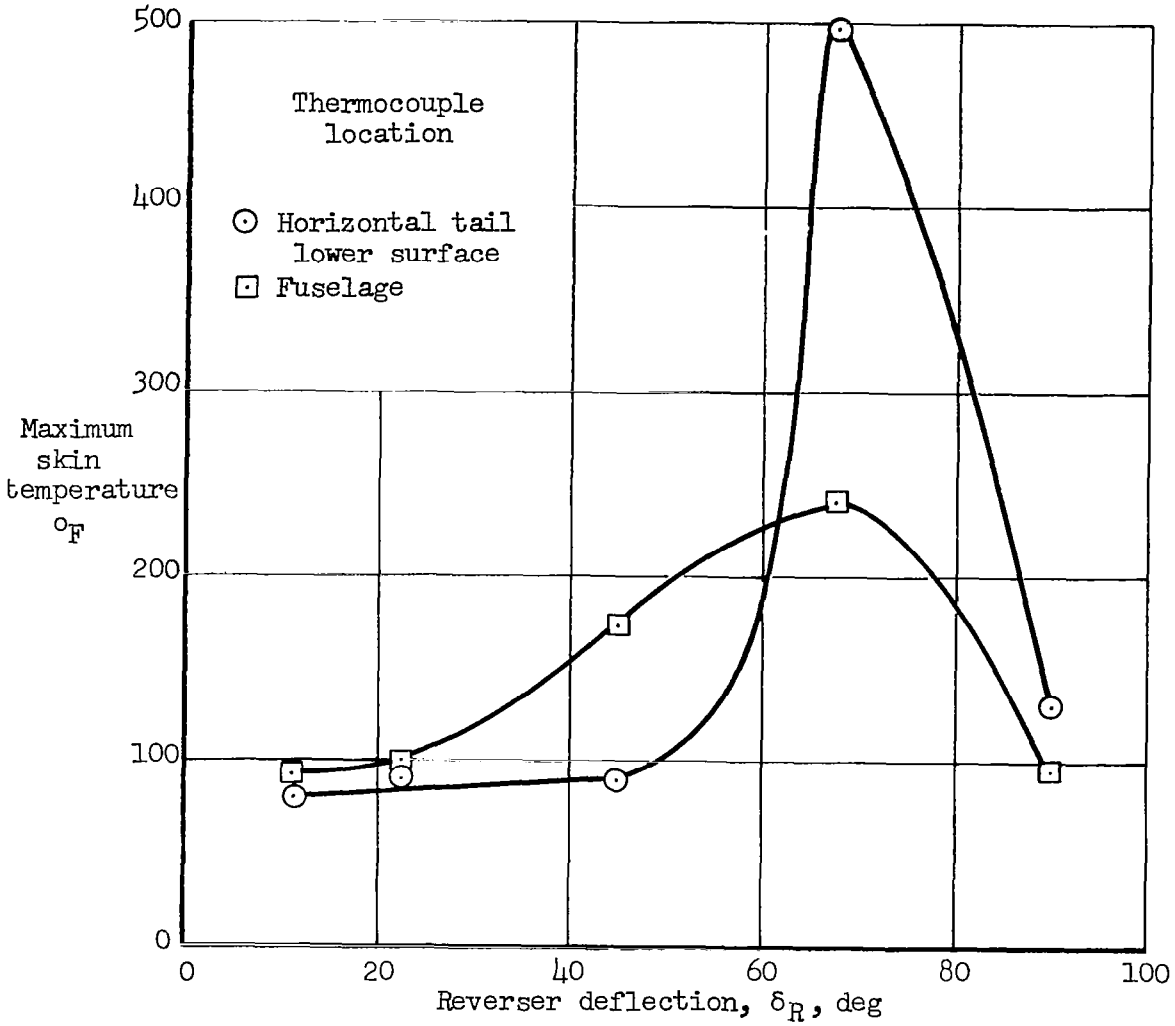

Figure 13.- Variation of maximum skin temperatures on the horizontal tail lower surface and fuselage with changes in reverser deflection angle; q_∞ = 35 psf, $\alpha = 0^\circ$, $i_t = 0^\circ$, $N/\sqrt{\theta} \approx 0.77$.

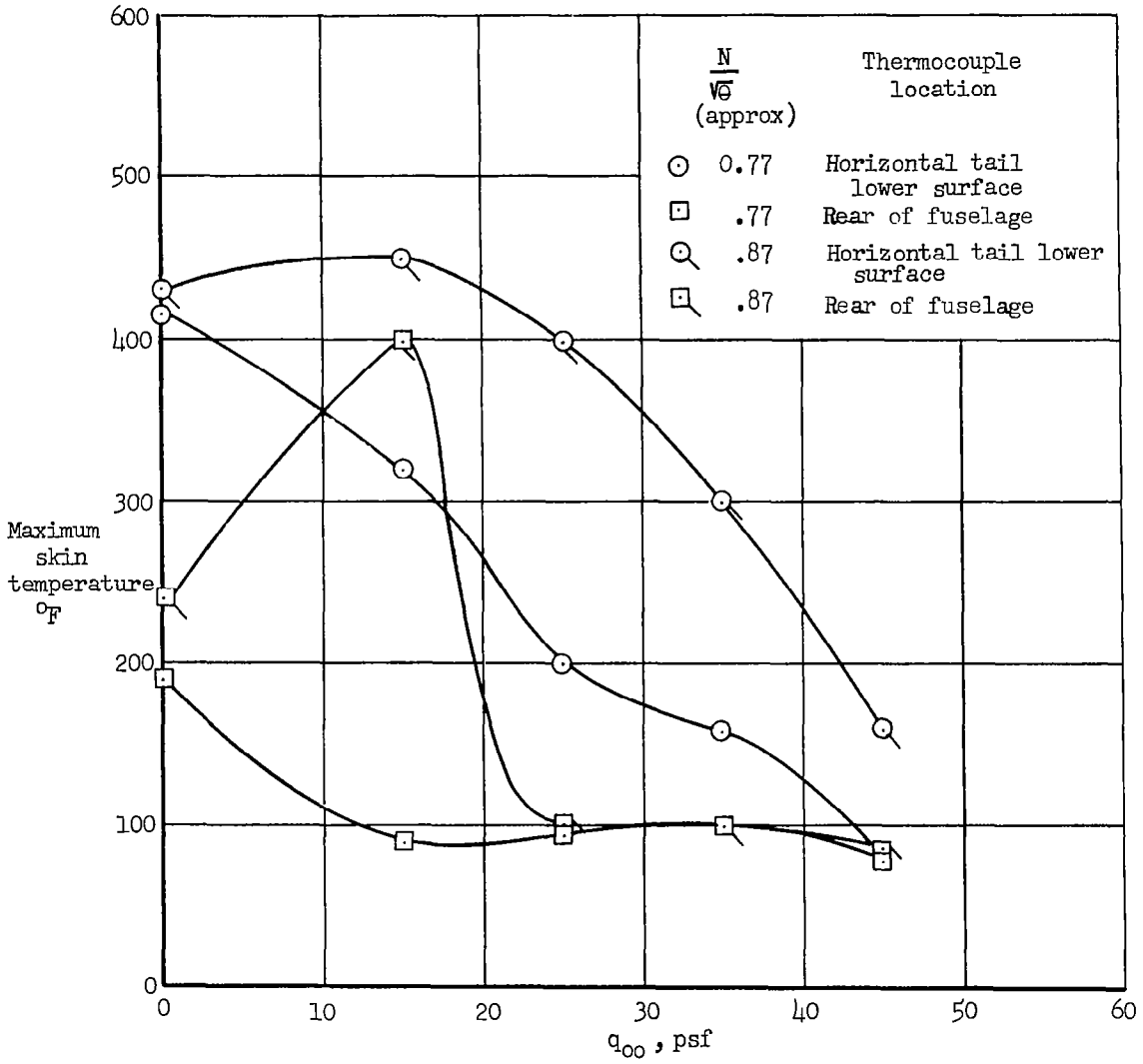

Figure 14.- Variation of maximum skin temperatures on the horizontal tail and fuselage with changes in q_{∞}; $\delta_R = 90^{\circ}$, $\alpha = 0^{\circ}$, $i_t = 0^{\circ}$.

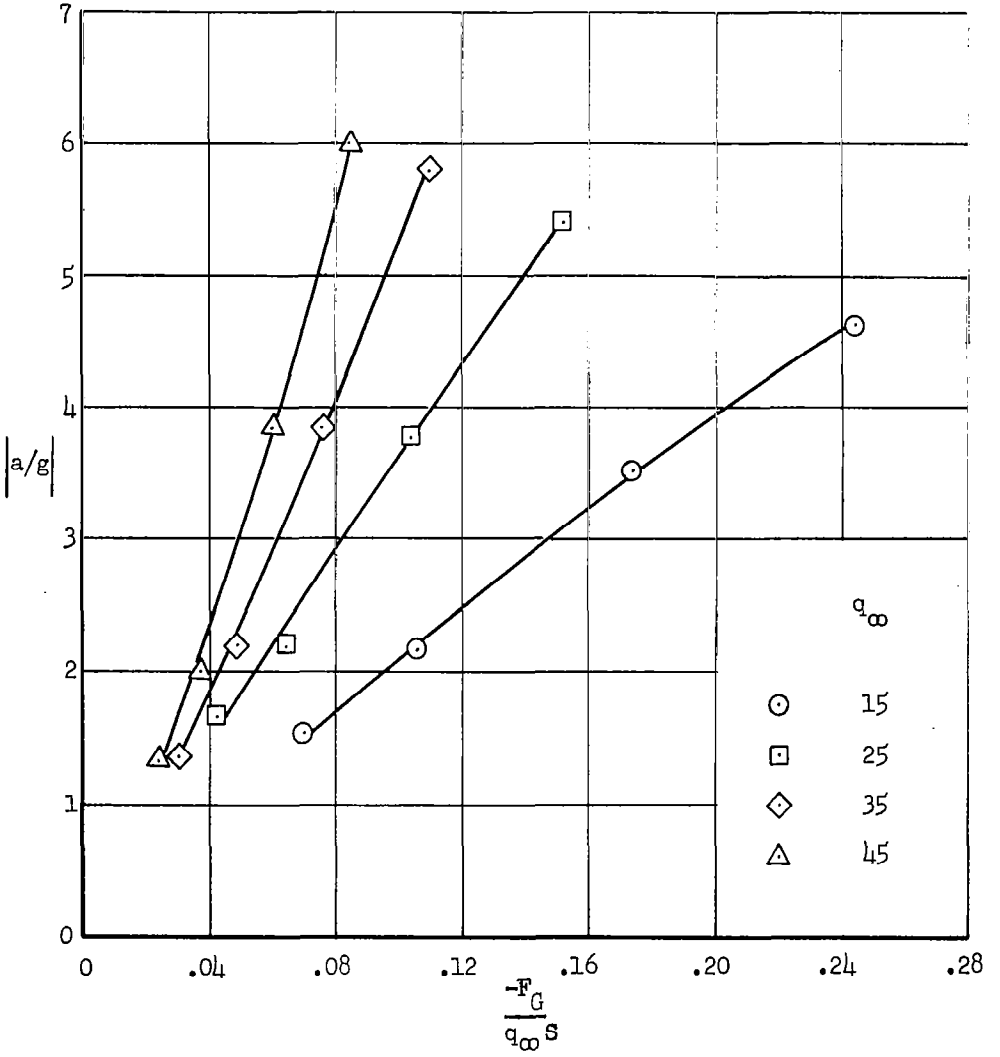

(a) Absolute values of acceleration maximums.

Figure 15.- Buffet accelerations on the horizontal tail at various q_∞; $\delta_R = 90^\circ$, $\alpha = 0^\circ$, $i_t = 0^\circ$.

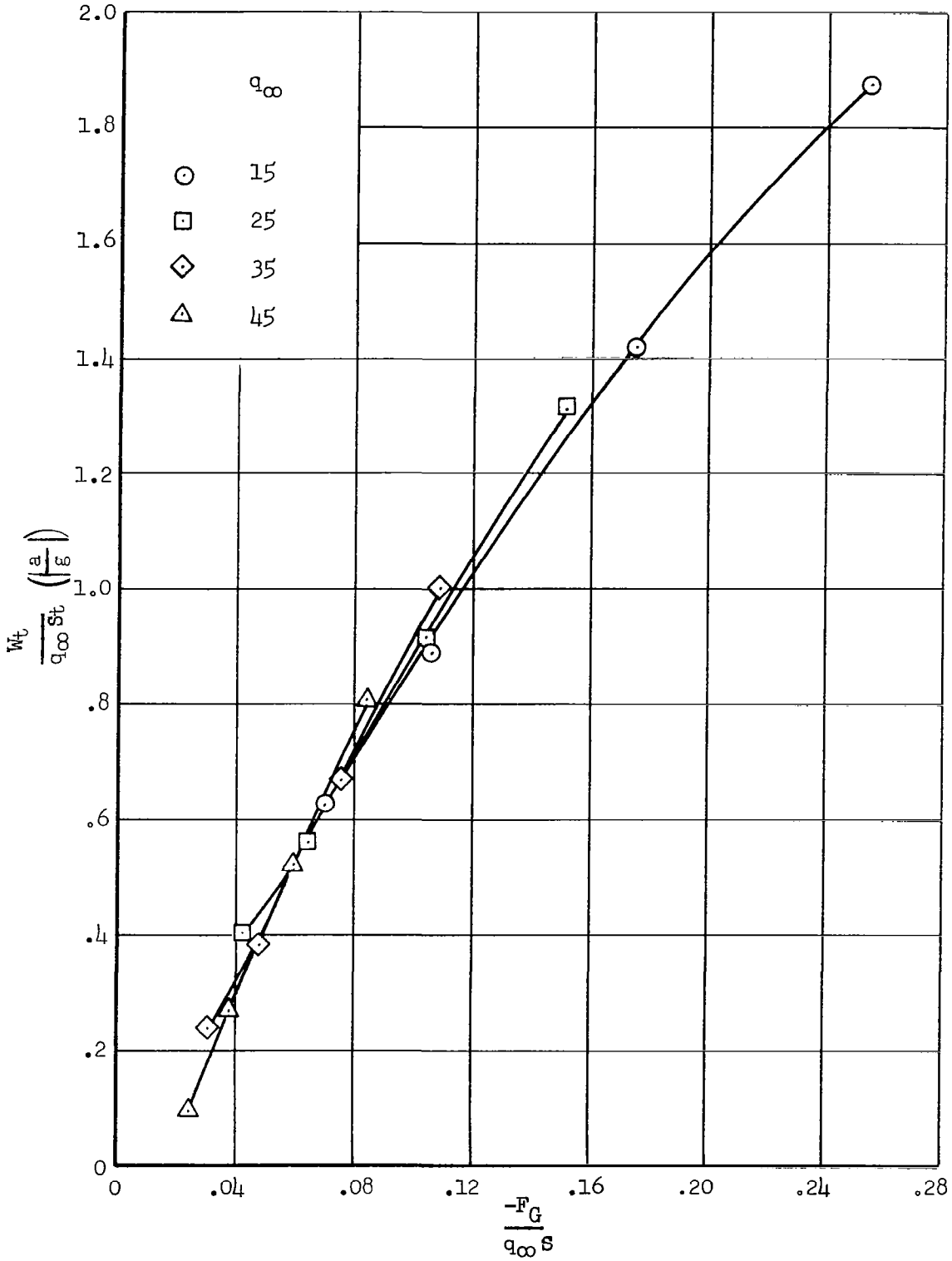

(b) Correlation derived from the parameter $(W_t/q_\infty S_t)(|a/g|)$.

Figure 15.- Concluded.